Regulation of the MLH1-MLH3 endonuclease in meiosis

Cannavo, Elda ; Sanchez, Aurore ; Anand, Roopesh ; Ranjha, Lepakshi ; Hugener, Jannik ; Adam, Céline ; Acharya, Ananya ; Weyland, Nicolas ; Aran-Guiu, Xavier ; Charbonnier, Jean-Baptiste ; Hoffmann, Eva R ; Borde, Valérie ; Matos, Joao ; Cejka, Petr

Abstract: During prophase of the first meiotic division, cells deliberately break their DNA1. These DNA breaks are repaired by homologous recombination, which facilitates proper chromosome segregation and enables the reciprocal exchange of DNA segments between homologous chromosomes2. A pathway that depends on the MLH1–MLH3 (MutL) nuclease has been implicated in the biased processing of meiotic recombination intermediates into crossovers by an unknown mechanism3,4,5,6,7. Here we have biochemically reconstituted key elements of this pro-crossover pathway. We show that human MSH4–MSH5 (MutS), which supports crossing over8, binds branched recombination intermediates and associates with MutL , stabilizing the ensemble at joint molecule structures and adjacent double-stranded DNA. MutS directly stimulates DNA cleavage by the MutL endonuclease. MutL activity is further stimulated by EXO1, but only when MutS is present. Replication factor C (RFC) and the proliferating cell nuclear antigen (PCNA) are additional components of the nuclease ensemble, thereby triggering crossing-over. Saccharomyces cerevisiae strains in which MutL cannot interact with PCNA present defects in forming crossovers. Finally, the MutL –MutS –EXO1–RFC–PCNA nuclease ensemble preferentially cleaves DNA with Holliday junctions, but shows no canonical resolvase activity. Instead, it probably processes meiotic recombination intermediates by nicking double-stranded DNA adjacent to the junction points9. As DNA nicking by MutL depends on its co-factors, the asymmetric distribution of MutS and RFC–PCNA on meiotic recombination intermediates may drive biased DNA cleavage. This mode of MutL nuclease activation might explain crossover-specific processing of Holliday junctions or their precursors in meiotic chromosomes4.

DOI: https://doi.org/10.1038/s41586-020-2592-2

Regulation of the MLH1-MLH3 endonuclease in meiosis

Elda Cannavo[1#], Aurore Sanchez[1#], Roopesh Anand[1#], Lepakshi Ranjha[1], Jannik Hugener[2], Céline Adam[3,4], Ananya Acharya[1,2], Nicolas Weyland[5], Xavier Aran-Guiu[6], Jean-Baptiste Charbonnier[7,8], Eva R. Hoffmann[6,9], Valérie Borde[3,4], Joao Matos[2] and Petr Cejka[1,2]

Affiliations:

[1]Institute for Research in Biomedicine, Università della Svizzera italiana (USI), Faculty of Biomedical Sciences, Switzerland

[2]Department of Biology, Institute of Biochemistry, Eidgenössische Technische Hochschule (ETH), Zürich, Switzerland

[3]Institut Curie, PSL Research University, CNRS UMR3244, Paris, France

[4]Paris Sorbonne Université, Paris, France

[5]Institute of Molecular Cancer Research, University of Zürich, Zürich, Switzerland

[6]Genome Damage and Stability Centre, School of Life Sciences, University of Sussex, Brighton, UK

[7]I2BC, iBiTec-S, CEA, CNRS UMR 9198, Université Paris-Sud, Gif-sur-Yvette, France;

[8]Université Paris Sud, Orsay, France

[9] DNRF Center for Chromosome Stability, Department of Cellular and Molecular Medicine, Faculty of Health and Medical Sciences, University of Copenhagen, Copenhagen, Denmark

[#] These authors contributed equally.

Materials & Correspondence: Petr Cejka, Institute for Research in Biomedicine, Via Vincenzo Vela 6, 6500 Bellinzona, Switzerland;

E-mail: petr.cejka@irb.usi.ch

SUMMARY

During prophase of the first meiotic division, cells deliberately break their DNA[1]. These DNA breaks are repaired by homologous recombination, which facilitates proper chromosome segregation and enables reciprocal exchange of DNA segments between homologous chromosomes, promoting thus genetic diversity in the progeny[2]. Genetic and cellular data implicated a pathway dependent on the MLH1-MLH3 (MutLγ) nuclease in the biased processing of meiotic recombination intermediates into crossovers, but mechanisms that lead its activation were unclear[3-7]. Here, we biochemically reconstituted key elements of this pro-crossover pathway. First, we show that human MSH4-MSH5 (MutSγ), which was known to support crossing over[8], binds branched recombination intermediates and physically associates with MutLγ. This helps stabilize the ensemble at joint molecule structures and adjacent dsDNA. Second, we show that MutSγ directly stimulates DNA cleavage by the MutLγ endonuclease, which demonstrates an unexpected direct function for MutSγ in triggering crossing-over. Third, we find that MutLγ activity is further stimulated by EXO1, but only when MutSγ is present. Fourth, we also identify the replication factor C (RFC) and the proliferating cell nuclear antigen (PCNA) as additional components of the nuclease ensemble, and show that *S. cerevisiae* strains expressing PCNA-interacting peptide (PIP) box-like mutated MutLγ present striking defects in forming crossovers. Finally, we show that the MutLγ-MutSγ-EXO1-RFC-PCNA nuclease ensemble preferentially cleaves DNA with Holliday junctions, but shows no canonical resolvase activity. Instead, the multilayered nuclease ensemble likely processes meiotic recombination intermediates by nicking dsDNA adjacent to the junction points[9]. Since DNA nicking by MutLγ is dependent on its co-factors, the asymmetric distribution of MutSγ and RFC-PCNA on meiotic recombination intermediates may drive biased DNA cleavage. This unique mode of MutLγ nuclease activation might explain crossover-specific processing of Holliday junctions within the meiotic chromosomal context[4].

MAIN TEXT

MutLγ is an ATP-stimulated endonuclease

To study human MutLγ (MLH1-MLH3), we expressed and purified the heterodimer from insect cells (Extended Data Fig. 1a,b). Similarly to the mismatch repair (MMR)-specific MutLα (MLH1-PMS2)[10] and yeast Mlh1-Mlh3[11,12], the human MLH1-MLH3 complex non-specifically nicked double-stranded supercoiled DNA (scDNA) with manganese as a metal co-factor (Fig. 1a, Extended Data Fig. 1c-e)[13]. Mutations in the conserved metal binding DQHA$(X)_2$E$(X)_4$E motif of MLH3 abolished the endonuclease, indicating that the DNA cleavage activity was intrinsic to the MutLγ heterodimer (Fig. 1a). ATP promoted the nuclease activity >2-fold (Fig. 1a, Extended Data Fig. 1f). Almost no nuclease activity was observed with magnesium (Extended Data Fig. 1g), which is believed to be the specific metal co-factor[10]. Experiments with various ATP analogs revealed that ATP hydrolysis by MLH1-MLH3 was required for the maximal stimulation of DNA cleavage (Extended Data Fig. 1h,i). The N-termini of both MLH1 and MLH3 proteins contain conserved Walker motifs implicated in ATP binding and hydrolysis[14]. To define whether the ATPase of MLH1, MLH3 or both subunits of the heterodimer promotes its nucleolytic activity, we prepared the respective hMutLγ variants with mutations in the ATPase motifs of either subunit individually or combined (Extended Data Fig. 1j,k)[14]. We observed that the integrity of the ATPase domain of MLH1, and to a much lesser degree of MLH3, promoted the nuclease activity of MLH1-MLH3 (Extended Data Fig. 1l,m). Without ATP, the ATPase-deficient variants of MLH1-MLH3 bound and cleaved DNA similarly as the wild type complex (Extended Data Fig. 1l-n). The MutLγ complex did not cleave oligonucleotide-based Holliday junctions (HJ) DNA (Extended Data Fig. 1o).

MutLγ and MutSγ bind to DNA junctions

Yeast and human MutLγ complexes bind DNA with a preference towards branched structures such as Holliday junctions[11,15]. Similarly, recombinant human MutSγ was shown to bind HJs[8]. We found that the human and yeast MutSγ complexes bound even better HJ precursors such as D-loops (Extended Data Fig.

2a-f). This binding preference agrees with the proposed early function of MutSγ to stabilize nascent strand invasion intermediates that mature into single-end invasions, which helps ensure their crossover designation[16]. In contrast, single-stranded DNA (ssDNA) or dsDNA was not bound by MutSγ (Extended Data Fig. 2b-f). Electrophoretic mobility shift assays demonstrated that the MutSγ and MutLγ complexes moderately stabilized each other at the DNA junctions (Extended Data Fig. 3a-e). Accordingly, the respective human or yeast MutSγ and MutLγ complexes directly physically interact (Fig. 1b and Extended Data Fig. 3f-h)[17]. The very slow migration of the protein-DNA complexes was indicative of multiple units of the heterocomplexes bound to the DNA substrate (Extended Data Fig. 3i,j), as shown previously for yeast MutLγ[11]. We note that the presence of DNA junctions was essential for stable DNA binding (Extended Data Fig. 3a,e), which supports a model where the branched DNA structure serves as a nucleation point for a MutSγ-MutLγ filament that then extends to the adjacent dsDNA arms[18].

MutSγ promotes the MutLγ nuclease

Previous *in vivo* experiments implicated MutSγ in the stabilization of nascent DNA joint molecules early in the meiotic pro-crossover pathway[8,17,19], but whether MutSγ is directly involved later in nucleolytic processing was not clear. Using our reconstituted system, we observed ~3-fold stimulation of the MLH1-MLH3 endonuclease by MSH4-MSH5 (Fig. 1c, Extended Data Fig. 4a-c), which was dependent on the MLH3 metal binding motif (Extended Data Fig. 4b). ATP promoted DNA cleavage by the MutSγ-MutLγ ensemble, and as in reactions with MutLγ alone, the maximal nuclease activity was observed when ATP hydrolysis was possible (Extended Data Fig. 4d). As MLH1 and MLH3, also MSH4 and MSH5 proteins contain conserved ATPase domains[14,16]. The ATP binding/hydrolysis motifs in MLH1 and MSH5 were both crucial, while the motif in MSH4 was less important and in MLH3 appeared dispensable (Fig. 1d,e, Extended Data Fig. 4e,f). The ATPase motif mutations in MSH4 or MSH5 instead did not affect the capacity of the two subunits to form a complex or bind DNA (Extended Data Fig. 4g,h). The stimulatory effect was likely facilitated by direct physical interactions between the cognate heterodimers, as yeast Msh4-Msh5 did not promote the nuclease activity of human MutLγ

(Extended Data Fig. 4i,j). MutSγ-MutLγ exhibited no detectable structure-specific nuclease or resolvase activity (Extended Data Fig. 4k,l).

To assess how the other human MutS homologue complexes, compared to MutSγ, promote the activity of MutLγ, we supplemented the MLH1-MLH3 nuclease reactions with the MMR factors MutSα (MSH2-MSH6) or MutSβ (MSH2-MSH3). MutSβ, but not hMutSα, could stimulate the MLH1-MLH3 nuclease to a similar level as MutSγ (Extended Data Fig. 5a-c)[13]. This agrees with previous experiments showing that yeast MutLγ could partially substitute MutLα in the repair of insertion/deletion mismatches in MMR[20]. These data also underpin the involvement of MutLγ in the metabolism of trinucleotide repeats linked to several neurodegenerative diseases, as well as rare MLH3 mutations found in patients with hereditary nonpolyposis colorectal cancer (HNPCC)/Lynch syndrome characterized by microsatellite instability[13,21,22].

EXO1 promotes the MutSγ-MutLγ nuclease

Genetic experiments with budding yeast revealed a structural (nuclease-independent) function of Exo1 in the Mlh1-Mlh3 pro-crossover pathway[5]. The effect was dependent on its direct interaction with the Mlh1 subunit of MutLγ[5,23], but it was unclear whether the interplay directly affects the Mlh3 endonuclease, and whether this function is conserved in higher eukaryotes. To test for the effect of EXO1 on the nuclease activity of MLH1-MLH3, we used the nuclease-deficient EXO1(DA) variant to prevent degradation of the resulting nicked DNA (Extended Data Fig. 6a). We observed no stimulation of the MLH1-MLH3 nuclease by EXO1(DA) alone, but EXO1(DA) promoted DNA cleavage ~2-3-fold when MSH4-MSH5 was present (Fig. 1f and Extended Data Fig. 6b,c). More than 40% DNA was cleaved using only 20 nM concentration of the multi-protein ensemble (Fig. 1f). In contrast to MSH4-MSH5 that moderately stabilized MLH1-MLH3 on DNA, we detected no such capacity of EXO1(DA) (Extended Data Fig. 6d). Yeast Exo1(DA) could not substitute human EXO1(DA) in the nuclease assays (Extended Data Fig. 6e), in agreement with a direct physical interaction between human EXO1(DA) and MLH1-MLH3 (Fig. 1g). Finally, EXO1(DA) did not promote the nuclease activity of MLH1-MLH3 with MutSβ (Extended Data Fig. 6f), indicating that EXO1 likely

158 specifically stimulates the endonuclease activity of MutSγ-MutLγ involved in mei-
159 otic recombination.
160
161 **PCNA promotes the MLH3 nuclease ensemble**
162 We next set out to test whether MLH1-MLH3 with its co-factors can catalyze DNA
163 cleavage under physiological conditions in magnesium. While almost no nuclease
164 activity of MLH1-MLH3 alone in magnesium was observed, weak nicking was seen
165 upon adding MSH4-MSH5, and the reactions were further stimulated by
166 EXO1(DA) (Fig. 2a). As RFC-PCNA are known to direct the MutLα endonuclease in
167 mismatch repair[10], we tested for their effect on MutLγ. Notably, we observed ad-
168 ditional ~2-fold stimulation of DNA cleavage when the RFC-PCNA complex was
169 included (Fig. 2a, Extended Data Fig. 7a-e). Nucleolytic cleavage was dependent
170 on the integrity of the MLH3 metal-binding motif (Extended Data Fig. 7b). Yeast
171 RFC could partially substitute for human RFC (Extended Data Fig. 7c), in accord
172 with the capacity of yeast RFC to load human PCNA on scDNA[10,24]. In contrast, no
173 stimulation was detected when RFC was omitted from the reaction mixture or
174 when using relaxed DNA (Extended Data Fig. 7b,f), indicating that PCNA must
175 likely be actively loaded onto scDNA by RFC[10,24]. No stimulation was observed
176 when using yeast instead of human PCNA (Extended Data Fig. 7b), or in reactions
177 with manganese (Extended Data Fig. 7g). Thus, while MutLγ on its own is a poor
178 nuclease that requires manganese, MutSγ, EXO1 and RFC-PCNA activate it to
179 cleave efficiently in a buffer containing physiological magnesium, and the reaction
180 is no longer stimulated by additional manganese (Fig. 2b).
181 RFC-PCNA could also promote the nuclease activity of MutLγ alone, although
182 to a lesser extent (Extended Data Fig. 7h), suggesting that MutSγ and EXO1(DA)
183 are not strictly required to mediate the stimulatory effect of RFC-PCNA. In accord,
184 we found that MutLγ directly physically interacts with PCNA (Fig. 2c). ATP was
185 necessary for the nuclease activity of the ensemble and for PCNA loading, and
186 could not be replaced by ADP or AMP-PNP, showing that ATP hydrolysis was re-
187 quired (Fig. 2d, Extended Data Fig. 7i). In contrast to the reactions in manganese,
188 the integrity of the ATPase motifs of all four MutSγ and MutLγ subunits was

189 required for maximal cleavage activity in magnesium (Fig. 2e, Extended Data Fig.
190 7j).

191 Notably, the nuclease ensemble preferentially cleaved plasmid-length DNA
192 with palindromic repeats forming a HJ-like structure (cruciform DNA, Fig. 2f), in
193 agreement with the binding preference of the MutSγ and MutLγ heterodimers to
194 these recombination intermediates (Extended Data Fig. 2b-f)[8,11,15]. However, the
195 activity of the complex on the cruciform DNA primarily yielded nicked products
196 (Fig. 2f), unlike canonical HJ resolvases that give rise to linear DNA upon con-
197 certed cleavage of both DNA strands at the junctions[25]. We also note that we did
198 not observe any cleavage of model HJ or D-loop oligonucleotide-based substrates
199 (Extended Data Fig. 7k). Our data suggest that the hMutLγ ensemble processes
200 recombination intermediates by resolution-independent nicking, in agreement
201 with results obtained from sequencing of heteroduplex DNA arising during meio-
202 sis in yeast cells, which indicated cleavage by nicking some distance away from
203 the DNA junction points[9].

204 Interactions with PCNA are often mediated by a PIP-box motif. We supple-
205 mented the MutLγ ensemble nuclease assays with a PIP-box peptide derived from
206 p21[26], or a control peptide with key residues mutated. The competing PIP-box
207 peptide eliminated the stimulatory effect of RFC-PCNA, while the control peptide
208 had no effect (Fig. 3a), demonstrating that the PCNA function in stimulating the
209 nuclease activity of the MutLγ ensemble is dependent on an interaction via a PIP-
210 box like motif. We next analyzed several mutants of conserved PIP-box-like se-
211 quences in MLH1, MLH3 and EXO1(DA)[27-29] (Fig. 3b). The respective mutations
212 did not notably affect the nuclease reactions *per se* without PCNA or the capacity
213 to bind DNA, but the mutants became partly refractory to stimulation by RFC-
214 PCNA, in particular when the PIP-box-like mutations of multiple factors were
215 combined (Fig. 3c, Extended Data Fig. 8a-e). Furthermore, the corresponding mu-
216 tations in the yeast homologues of Mlh1 and Mlh3 (Fig. 3b) resulted in meiotic
217 defects, as indicated by a decrease in the frequency of crossovers at the *CEN8-*
218 *THR1* interval leading to chromosome non-disjunction and reduced spore viabil-
219 ity (Fig. 3d,e, Extended Data Fig. 9a). We noted that the stability of Mlh1^{P} was re-
220 duced *in vivo*, which may contribute to the very severe phenotype, but the levels
221 of Mlh3^{P} were comparable to wild type (Extended Data Fig. 9b,c). We also found

yeast Mlh1 and Mlh3 as a part of a complex with Rfc1 in meiotic cells at the time of joint molecule resolution (Extended Data Fig. 9d). Finally, using chromatin immunoprecipitation and synchronous meiotic yeast cultures, we observed an enrichment of Rfc1 at both natural and engineered DSB hotspots in late meiotic prophase at the time when joint molecules are resolved into crossovers (Fig. 3f). This coincides with the accumulation of Mlh3 at the same hotspots[30]. The accumulation of Rfc1 at sites of recombination was independent of Mlh3, suggesting that it may be retained from an earlier step of DNA synthesis (Extended Data Fig. 9e).

We demonstrated here that MutSγ, EXO1 and RFC-PCNA are required to activate the nuclease activity of MutLγ under physiological conditions with magnesium, but we failed to detect any canonical HJ resolvase activity. Rather, our data suggest that the nuclease ensemble processes meiotic joint molecule intermediates by biased resolution-independent nicking of dsDNA in the vicinity of HJs. Since HJs are symmetric and their resolution can yield both crossovers and non-crossovers[25], how is the crossover bias established? As MutSγ likely stabilizes asymmetric HJ precursors, it may be asymmetrically distributed at the mature joint molecules containing HJs (Extended Data Fig. 10). Similarly, PCNA is likely loaded asymmetrically at joint molecules to facilitate DNA synthesis by polymerase δ, or at strand discontinuities before the ligation of double HJs takes place. We propose that the asymmetric presence of the MutLγ nuclease co-factors might provide the signal to guarantee biased, crossover-specific processing of meiotic joint molecule intermediates (Extended Data Fig. 10). In this model the MMR reaction that limits mutagenesis during DNA replication[11] is repurposed in meiotic recombination to instead promote diversity among the recombined DNA molecules.

REFERENCES

1 Keeney, S., Giroux, C. N. & Kleckner, N. Meiosis-specific DNA double-strand breaks are catalyzed by Spo11, a member of a widely conserved protein family. *Cell* **88**, 375-384 (1997).

2 Hunter, N. Meiotic Recombination: The Essence of Heredity. *Cold Spring Harb Perspect Biol* **7**, doi:10.1101/cshperspect.a016618 (2015).

3 Nishant, K. T., Plys, A. J. & Alani, E. A mutation in the putative MLH3 endonuclease domain confers a defect in both mismatch repair and meiosis in Saccharomyces cerevisiae. *Genetics* **179**, 747-755, doi:10.1534/genetics.108.086645 (2008).
4 Zakharyevich, K., Tang, S., Ma, Y. & Hunter, N. Delineation of joint molecule resolution pathways in meiosis identifies a crossover-specific resolvase. *Cell* **149**, 334-347, doi:10.1016/j.cell.2012.03.023 (2012).
5 Zakharyevich, K. *et al.* Temporally and biochemically distinct activities of Exo1 during meiosis: double-strand break resection and resolution of double Holliday junctions. *Mol Cell* **40**, 1001-1015, doi:10.1016/j.molcel.2010.11.032 (2010).
6 De Muyt, A. *et al.* BLM helicase ortholog Sgs1 is a central regulator of meiotic recombination intermediate metabolism. *Mol Cell* **46**, 43-53, doi:10.1016/j.molcel.2012.02.020 (2012).
7 Svetlanov, A., Baudat, F., Cohen, P. E. & de Massy, B. Distinct functions of MLH3 at recombination hot spots in the mouse. *Genetics* **178**, 1937-1945, doi:10.1534/genetics.107.084798 (2008).
8 Snowden, T., Acharya, S., Butz, C., Berardini, M. & Fishel, R. hMSH4-hMSH5 recognizes Holliday Junctions and forms a meiosis-specific sliding clamp that embraces homologous chromosomes. *Mol Cell* **15**, 437-451, doi:10.1016/j.molcel.2004.06.040 (2004).
9 Marsolier-Kergoat, M. C., Khan, M. M., Schott, J., Zhu, X. & Llorente, B. Mechanistic View and Genetic Control of DNA Recombination during Meiosis. *Mol Cell* **70**, 9-20 e26, doi:10.1016/j.molcel.2018.02.032 (2018).
10 Kadyrov, F. A., Dzantiev, L., Constantin, N. & Modrich, P. Endonucleolytic function of MutLalpha in human mismatch repair. *Cell* **126**, 297-308, doi:10.1016/j.cell.2006.05.039 (2006).
11 Ranjha, L., Anand, R. & Cejka, P. The Saccharomyces cerevisiae Mlh1-Mlh3 heterodimer is an endonuclease that preferentially binds to Holliday junctions. *J Biol Chem* **289**, 5674-5686, doi:10.1074/jbc.M113.533810 (2014).
12 Rogacheva, M. V. *et al.* Mlh1-Mlh3, a meiotic crossover and DNA mismatch repair factor, is a Msh2-Msh3-stimulated endonuclease. *J Biol Chem* **289**, 5664-5673, doi:10.1074/jbc.M113.534644 (2014).
13 Kadyrova, L. Y., Gujar, V., Burdett, V., Modrich, P. L. & Kadyrov, F. A. Human MutLgamma, the MLH1-MLH3 heterodimer, is an endonuclease that promotes DNA expansion. *Proc Natl Acad Sci U S A* **117**, 3535-3542, doi:10.1073/pnas.1914718117 (2020).
14 Sonntag Brown, M., Lim, E., Chen, C., Nishant, K. T. & Alani, E. Genetic analysis of mlh3 mutations reveals interactions between crossover promoting factors during meiosis in baker's yeast. *G3 (Bethesda)* **3**, 9-22, doi:10.1534/g3.112.004622 (2013).
15 Claeys Bouuaert, C. & Keeney, S. Distinct DNA-binding surfaces in the ATPase and linker domains of MutLgamma determine its substrate specificities and exert separable functions in meiotic recombination and mismatch repair. *PLoS Genet* **13**, e1006722, doi:10.1371/journal.pgen.1006722 (2017).
16 Nishant, K. T., Chen, C., Shinohara, M., Shinohara, A. & Alani, E. Genetic analysis of baker's yeast Msh4-Msh5 reveals a threshold crossover level for meiotic viability. *PLoS Genet* **6**, doi:10.1371/journal.pgen.1001083 (2010).

17 Santucci-Darmanin, S. *et al.* The DNA mismatch-repair MLH3 protein interacts with MSH4 in meiotic cells, supporting a role for this MutL homolog in mammalian meiotic recombination. *Hum Mol Genet* **11**, 1697-1706 (2002).
18 Manhart, C. M. *et al.* The mismatch repair and meiotic recombination endonuclease Mlh1-Mlh3 is activated by polymer formation and can cleave DNA substrates in trans. *PLoS Biol* **15**, e2001164, doi:10.1371/journal.pbio.2001164 (2017).
19 Kneitz, B. *et al.* MutS homolog 4 localization to meiotic chromosomes is required for chromosome pairing during meiosis in male and female mice. *Genes Dev* **14**, 1085-1097 (2000).
20 Flores-Rozas, H. & Kolodner, R. D. The Saccharomyces cerevisiae MLH3 gene functions in MSH3-dependent suppression of frameshift mutations. *Proc Natl Acad Sci U S A* **95**, 12404-12409 (1998).
21 Lipkin, S. M. *et al.* MLH3: a DNA mismatch repair gene associated with mammalian microsatellite instability. *Nat Genet* **24**, 27-35, doi:10.1038/71643 (2000).
22 Wu, Y. *et al.* A role for MLH3 in hereditary nonpolyposis colorectal cancer. *Nat Genet* **29**, 137-138, doi:10.1038/ng1001-137 (2001).
23 Dherin, C. *et al.* Characterization of a highly conserved binding site of Mlh1 required for exonuclease I-dependent mismatch repair. *Mol Cell Biol* **29**, 907-918, doi:10.1128/MCB.00945-08 (2009).
24 Pluciennik, A. *et al.* PCNA function in the activation and strand direction of MutLalpha endonuclease in mismatch repair. *Proc Natl Acad Sci U S A* **107**, 16066-16071, doi:10.1073/pnas.1010662107 (2010).
25 Rass, U. *et al.* Mechanism of Holliday junction resolution by the human GEN1 protein. *Genes Dev* **24**, 1559-1569, doi:10.1101/gad.585310 (2010).
26 Bruning, J. B. & Shamoo, Y. Structural and thermodynamic analysis of human PCNA with peptides derived from DNA polymerase-delta p66 subunit and flap endonuclease-1. *Structure* **12**, 2209-2219, doi:10.1016/j.str.2004.09.018 (2004).
27 Lee, S. D. & Alani, E. Analysis of interactions between mismatch repair initiation factors and the replication processivity factor PCNA. *J Mol Biol* **355**, 175-184, doi:10.1016/j.jmb.2005.10.059 (2006).
28 Liberti, S. E. *et al.* Bi-directional routing of DNA mismatch repair protein human exonuclease 1 to replication foci and DNA double strand breaks. *DNA Repair (Amst)* **10**, 73-86, doi:10.1016/j.dnarep.2010.09.023 (2011).
29 Genschel, J. *et al.* Interaction of proliferating cell nuclear antigen with PMS2 is required for MutLalpha activation and function in mismatch repair. *Proc Natl Acad Sci U S A* **114**, 4930-4935, doi:10.1073/pnas.1702561114 (2017).
30 Sanchez, A. A., C; Rauh, F; Duroc, Y; Ranjha, L; Lombard, B; Mu, X; Loew, D; Keeney, S; Cejka, P; Guérois R; Klein F; Charbonnier, JB; Borde, V. Mechanism of in vivo activation of the MutLγ-Exo1 complex for meiotic crossover formation. *bioRxiv* **2019.12.16.876623**, doi:https://doi.org/10.1101/2019.12.16.876623 (2019).

352 **FIGURE LEGENDS**

353

354 **Figure 1. MSH4-MSH5 and EXO1(DA) interact with and promote the MLH1-**
355 **MLH3 endonuclease. a**, Top, alignment of the metal binding motif in MLH3. Con-
356 served residues are highlighted in red. Substitution mutations used in this study
357 are in italics. Bottom, nuclease assays with MLH1-MLH3 and 2.7 kbp-long scDNA,
358 with 5 mM manganese acetate, without or with 0.5 mM ATP, at 37 °C. **b**, Protein
359 interaction assays with immobilized MSH4-MSH5 (bait, 220 nM) and MLH1-
360 MLH3 (prey). The 10% polyacrylamide gel was stained with silver. **c**, Nuclease
361 assays with MutSγ and MutLγ (5 mM manganese acetate, 30 °C, 0.5 mM ATP). Av-
362 erages shown; n=3; error bars, SEM. **d**, Top, alignment of MSH5 and MSH4 ATPase
363 domains. Conserved residues are highlighted in red. Alanine substitutions used in
364 this study are in italics. Bottom, nuclease assays with MutSγ ATPase variants (5
365 mM manganese acetate, 30 °C, 0.5 mM ATP). Averages shown; error bars, SEM;
366 n=3. **e**, Top, alignment of MLH1 and MLH3 ATPase domains. Conserved residues
367 are highlighted in red. Alanine substitutions used in this study are in italics. Bot-
368 tom, nuclease assays with MutLγ ATPase variants (5 mM manganese acetate, 30
369 °C, 0.5 mM ATP). Averages shown; error bars, SEM; n=3. **f**, Quantitation of kinetic
370 nuclease assays with MutSγ and MutLγ, without or with nuclease-deficient
371 EXO1(DA)(20 nM). The assays were carried out at 30 °C with 5 mM manganese
372 acetate and 2 mM ATP. Averages shown; error bars, SEM; n=3. **g**, Protein interac-
373 tion assays with immobilized MutLγ (bait) and EXO1 (prey). The 10% polyacryla-
374 mide gel was stained with silver.

375

376 **Figure 2. RFC-PCNA promote DNA cleavage by the MutLγ-MutSγ-EXO1(DA)**
377 **ensemble. a**, Nuclease assays with 5.6 kbp-long scDNA and indicated human pro-
378 teins was carried out with 5 mM magnesium acetate and 2 mM ATP at 37 °C. A
379 representative experiment is shown at the bottom, a quantitation (averages
380 shown; n=7; error bars, SEM) at the top. **b**, Representative nuclease assays carried
381 out with 5 mM magnesium acetate, 5 mM manganese acetate or 5/1 mM magne-
382 sium/manganese acetate, respectively, as indicated, with indicated proteins, con-
383 taining 2 mM ATP and incubated at 37 °C. **c**, Protein interaction assays with

immobilized MLH1-MLH3 (bait) and PCNA (prey). The 10% polyacrylamide gel was stained with silver. **d**, Nuclease reactions as in panel a, lane 5, but either without ATP, with ATP or with non-hydrolysable AMP-PNP (2 mM). Averages shown; error bars, SEM; n=4. **e**, Nuclease reactions with MLH1-MLH3 (50 nM), MSH4-MSH5 (50 nM), EXO1(DA) (50 nM) and yRFC-hPCNA (50-100 nM, respectively), lane 2. Lanes 3-7 contain instead MLH1-MLH3 or MSH4-MSH5 variants (50 nM) deficient in ATP hydrolysis, as indicated. See schemes in Fig. 1d,e for the specific mutations. Reactions were carried out with 5 mM magnesium acetate and 2 mM ATP at 37 °C. Averages shown; error bars, SEM; n=4. **f**, Representative nuclease reactions with MLH1-MLH3, MSH4-MSH5, EXO1(DA) and yRFC-hPCNA, as indicated, with 3.5 kbp-long dsDNA either containing (left) or not (right) DNA repeat forming HJ-like cruciform DNA. Averages shown; error bars, SEM; n=9.

Figure 3. The stimulation of the MLH3 nuclease ensemble by PCNA requires a PIP box motif and is conserved in evolution. **a**, Nuclease assays with MLH1-MLH3, MSH4-MSH5, EXO1(DA), and yRFC-hPCNA, as indicated, with 5 mM magnesium acetate and 2 mM ATP at 37 °C. The reactions were supplemented with a p21 PIP-box wild type or mutated control peptide, where indicated (670 nM, ~5-fold over K_d of wild type peptide for PCNA)[26]. Averages shown; error bars, SEM; n=4. **b**, Alignment of PIP-box-like motifs from various human or *S. cerevisiae* proteins. Residues more likely to be conserved are highlighted in red. Wild type human and yeast EXO1, MLH3/Mlh3 and MLH1/Mlh1 were mutated to create respective (^{P}) variants with indicated residue substitutions (*A* in italics). **c**, Nuclease assays with MLH1-MLH3, MSH4-MSH5, EXO1(DA), and yRFC-hPCNA, as indicated, with 5 mM magnesium acetate and 2 mM ATP at 37 °C. Where indicated, wild type MLH1 was replaced with MLH1^P (Q562A-I565A-F568A), wild type MLH3 with MLH3^P (Q341A-V344A-F347A), and EXO1(DA), with EXO1(DA)^P (D173A-Q788A-L791A). Averages shown; error bars, SEM, n=5. **d**, Recombination frequency, expressed as a map distance in centimorgans, was assayed in the wild type *S. cerevisiae* strain, *mlh1*Δ and *mlh3*Δ, and in strains complemented with an untagged construct expressing wild type Mlh1, Mlh1^P (Q572A-L575A-F578A) or Mlh3^P (Q293A-V296A-F300A). All variants were expressed from the endogenous gene locus. Averages shown; error bars, SD; n≥900 from 3 independent

experiments. **e**, Frequency of chromosome VIII non-disjunction in strains as described in panel d. Averages shown; error bars, SD; n≥900 from 3 independent experiments. **f**, Rfc1-TAP levels at the indicated meiotic DSB hotspots relative to a negative control site (*NFT1)* were assessed by ChIP and qPCR during a meiotic time-course (synchronized *pCUP1-IME1* cells). Averages shown; error bars, SD; n=2. The cartoon illustrates the position of sites analyzed by qPCR relative to the meiotic chromosome structure.

METHODS

Preparation of expression vectors

To prepare the MSH4-MSH5 expression vector, the MSH4-STREP and MSH5-8xHIS constructs were codon-optimized for expression in *Spodoptera frugiperda Sf*9 cells and synthesized (GenScript). The genes were amplified by PCR using M13 forward and reverse primers (see Supplementary Data Table 1 for sequences of all oligonucleotides) and digested with *Sal*I and *Hin*dIII (for MSH4) or *Sma*I and *Kpn*I (for MSH5) restriction endonucleases (New England Biolabs). Digested fragments were ligated into corresponding sites in pFBDM (Addgene) to obtain pFBDM-hMSH4co-STREP and pFBDM-hMSH5co-HIS, respectively. Both plasmids were then digested with *Bam*HI and *Hin*dIII (New England Biolabs) and ligated to generate pFBDM-hMSH4co-STREP-hMSH5co-HIS. To prepare expression constructs coding for the ATPase variants of hMSH4 and hMSH5, the respective conserved residues in the Walker A motifs (see ref[16]) were mutated by QuikChange II site-directed mutagenesis kit (Agilent Technologies). To prepare MSH4G685A, the pFB-hMSH4co-STREP-hMSH5co-HIS vector was mutated with primers HMSH4G685A_FO and HMSH4G685A_RE. This created pFB-hMSH4coG685A-STREP-hMSH5co-HIS. To prepare MSH5G597A, HMSH5G597A_FO and HMSH5G597A_RE primers were used to create pFB-hMSH4co-STREP-hMSH5coG597A-HIS. We also prepared a construct combining both mutations, but the resulting mutant complex was not stable and could not be purified.

To prepare the MLH1 and MLH3 expression vectors, both genes were amplified by PCR from pFL-his-MLH3co-MLH1co containing both *MLH1* and *MLH3* genes, which were codon-optimized for insect cell expression. To amplify *MLH1*, FLAG-hMLH1co_FO and hMLH1co_RE primers were used. The PCR product was digested with *Nhe*I and *Xba*I (New England Biolabs) and inserted in pFB-MBP-MLH3-his[11] creating pFB-FLAG-hMLH1co (the sequence of *MLH3* was removed during this step). Similarly, MLH3 was amplified using MLH3co_FO and MLH3co_RE. The PCR product was digested with *Nhe*I and *Xma*I (New England Biolabs) and inserted into pFB-MBP-MLH3-HIS, generating pFB-MBP-hMLH3co. The sequence of non-optimized *MLH3* was removed during this step. The consensus metal-binding motif in MLH3 is DQHAADE (conserved residues

underlined)[3,10]. To prepare the nuclease-dead variant, the sequence of wild type *MLH3* in pFB-MBP-MLH3co-HIS was mutated using primers HMLH33ND_FO and HMLH33ND_RE. This created a sequence with 3 point mutations including D1223N, Q1224K and E1229K (*NK*HAAD*K*, mutated residues in italics), and the resulting vector was pFB-MBP-MLH3co3ND-HIS. To disrupt the ATPase of hMLH1[14], the pFB-FLAG-hMLH1co was mutated using primers HMLH1E34A_FO and HMLH1E34A_RE. This created pFB-FLAG-MLH1E34A. To mutate the corresponding conserved residue in MLH3, the pFB-HIS-MBP-MLH3co was mutated using primers HMLH3E28A_FO and HMLH3E28A_RE. This created pFB-HIS-MBP-MLH3E28A. To prepare the MLH1^{P} variant, the pFB-FLAG-hMLH1co plasmid was mutated using HMLH1_PIP1_3AFO and HMLH1_PIP1_3ARE primers. To prepare the MLH3^{P} variant, the pFB-FLAG-hMLH3co plasmid was mutated using HMLH3_PIP_3AFO and HMLH3_PIP_3ARE primers.

To prepare pFB-hEXO1-FLAG, the sequence coding for wild type human EXO1 (or EXO1[DA], containing the D173A mutation inactivating its nuclease) was amplified by PCR using primers HEXO1_FO and HEXO1_RE, and respective vectors (a kind gift from Stefano Ferrari, University of Zurich)[31] as templates. The PCR products were digested by *Bam*HI and *Xma*I (New England Biolabs), and cloned into corresponding sites in pFB-MBP-Sae2-HIS[32] (the sequence of MBP-Sae2 was removed during the process, FLAG-tag was added to the C-terminus and a HIS-tag from the original construct was not translated due to a Stop codon).

To prepare pFB-hMSH2-FLAG, the sequence coding for MSH2 was amplified from pFB-hMSH2[33] using primers HMSH2FLAG_FO and HMSH2FLAG_RE. The PCR product was digested by *Bam*HI and *Xho*I (New England Biolabs), and cloned into corresponding sites in pFB-MBP-Sae2 (the sequence of MBP-Sae2 was removed during the process, FLAG-tag was added to the C-terminus of MSH2 and a HIS-tag from the original construct was not translated due to a Stop codon).

To prepare pFB-HIS-yMLH1, pFB-GST-yMLH1[11] was digested using *Bam*HI (New England Biolabs) to remove the GST tag. This procedure left behind a single *Bam*HI site. Two complementary oligonucleotides His-For and His-Rev were annealed to each other, and cloned into the *Bam*HI site. This introduced a sequence coding for 8xHIS tag before the yeast *MLH1* gene creating pFB-HIS-yMLH1.

To prepare pFB-MBP-yMLH3, a termination codon was introduced after the yMLH3 gene in pFB-MBP-yMLH3-HIS[11] so that the HIS-tag would not be translated with the yMlh3 protein. This was carried out by site-directed mutagenesis using forward primer 329 and reverse primer 330.

To prepare the expression vector for yeast Msh4, the yeast *MSH4* gene was amplified from the genomic DNA of the *S. cerevisiae* SK1 strain using forward primer 258 and reverse primer 259b. The reverse primer introduced the sequence for the C-terminal STREP affinity tag. The amplified product was digested with *Bam*HI and *Hin*dIII (New England Biolabs) and cloned into corresponding sites of pFB-GST-MLH1[11] to create pFB-yMSH4-STREP. The yeast *MSH5* gene was amplified from the genomic DNA of the *S. cerevisiae* W303 strain using forward primer 265 and reverse primer 266. The *MSH5* gene was then cloned into *Bam*HI and *Xho*I restriction sites of pFB-MBP-MLH3-HIS[11] to create pFB-yMSH5-HIS.

Purification of human MLH1-MLH3

The bacmids and baculoviruses were prepared individually using pFB-FLAG-hMLH1co and pFB-HIS-MBP-hMLH3co vectors according to manufacturer's instructions (Bac-to-Bac system, Life Technologies). *Spodoptera frugiperda* 9 (*Sf*9) cells were seeded at 500,000 cells per ml 16 h before infection. The cells were then co-infected with both baculoviruses and incubated for 52 h at 27 °C with constant agitation. The cells were then harvested (500 x g, 10 min) and washed once with PBS (137 mM NaCl, 2.7 mM KCl, 10 mM Na_2HPO_4, 1.8 mM KH_2PO_4). The pellets were snap-frozen in liquid nitrogen and stored at -80 °C. All subsequent steps were carried out on ice or at 4 °C. The pellets were resuspended in 3 volumes of lysis buffer [50 mM Tris-HCl pH 7.5, 1 mM dithiothreitol (DTT), 1 mM ethylenediaminetetraacetic acid (EDTA), 1 mM phenylmethylsulfonyl fluoride (PMSF), 1:400 (volume/volume) protease inhibitor cocktail (Sigma, P8340), 30 µg/ml leupeptin (Merck)] and incubated for 20 min with continuous stirring. Next, 1/2 volume of 50% glycerol was added, followed by 6.5% volume of 5 M NaCl (final concentration 305 mM). The suspension was further incubated for 30 min with continuous stirring. The cell suspension was centrifuged for 30 min at 48,000 x g to obtain soluble extract. The supernatant was transferred to tubes containing pre-equilibrated Amylose resin (New England Biolabs, 4 ml per 1 l of

*Sf*9 culture) and incubated for 1 h with continuous agitation. The resin was collected by spinning at 2,000 x g for 2 min and washed extensively batchwise and on a disposable column (10 ml, Thermo Fisher) with Amylose wash buffer [50 mM Tris-HCl pH 7.5, 1 mM β-mercaptoethanol (β-ME), 1 mM PMSF, 10% glycerol, 300 mM NaCl]. Protein was eluted with Amylose elution buffer [50 mM Tris-HCl pH 7.5, 0.5 β-ME, 1 mM PMSF, 10% glycerol, 300 mM NaCl, 10 mM maltose (Sigma)] and the total protein concentration was estimated by Bradford assay. To cleave off the maltose binding tag (MBP), 1/6 (weight/weight) of PreScission protease (PP)[34], with respect to total protein concentration in the eluate, was added and incubated for 1 h. Next, the cleaved amylose eluate was diluted by adding 1/2 volume of FLAG dilution buffer (50 mM Tris-HCl pH 7.5, 1 mM PMSF, 10% glycerol, 300 mM NaCl) to lower the concentration of β-ME. The diluted eluate was then incubated batchwise for 1 h with pre-equilibrated anti-FLAG M2 affinity resin (Sigma, A2220, 0.8 ml). The resin was washed extensively with FLAG wash buffer (50 mM Tris-HCl pH 7.5, 0.5 mM β-ME, 1 mM PMSF, 10% glycerol, 150 mM NaCl). Protein was eluted with FLAG wash buffer containing 150 ng/µl 3x FLAG peptide (Sigma), aliquoted, frozen in liquid nitrogen and stored at -80 °C. The final construct contained a FLAG tag at the N-terminus of MLH1. The yield from 1 l culture was ~0.5 mg and the concentration ~2 µM. All MLH1-MLH3 mutants were expressed and purified using the same procedure.

Purification of human MSH4-MSH5

The human MSH4-MSH5 complex was expressed from a dual pFB-hMSH4co-STREP-hMSH5co-HIS vector in *Sf*9 cells using the Bac-to-Bac system as described above. All purification steps were carried out on ice or at 4 °C. The cell pellets were resuspended in 3 volumes of nickel-nitriloacetic acid (NiNTA) lysis buffer [50 mM Tris-HCl pH 7.5, 2 mM β-ME, 1 mM PMSF, 1:400 (volume/volume) protease inhibitor cocktail (Sigma, P8340), 30 µg/ml leupeptin (Merck), 20 mM imidazole] and incubated for 20 min with continuous stirring. Next 1/2 volume of 50% glycerol was added, followed by 6.5% volume of 5 M NaCl (final concentration 305 mM), and the suspension was further incubated for 30 min with continuous stirring. To obtain soluble extract, the suspension was centrifuged at 48,000 x g for 30 min. The soluble extract was transferred to a tube containing pre-

equilibrated NiNTA resin (Qiagen, 4 ml per 1 l *Sf*9 cells) and incubated for 1 h with continuous mixing. The NiNTA resin was collected by centrifugation at 2,000 x g for 2 min. The resin was washed extensively batchwise and on a disposable column with NiNTA wash buffer (50 mM Tris-HCl pH 7.5, 2 mM β-ME, 300 mM NaCl, 1 mM PMSF, 10% glycerol, 20 mM imidazole). Protein was eluted with NiNTA wash buffer containing 250 mM imidazole. The eluted sample was incubated with pre-equilibrated Strep-Tactin Superflow resin (Qiagen, 0.7 ml) for 90 min with continuous mixing. The resin was transferred to a disposable column and washed extensively with Strep wash buffer (50 mM Tris-HCl pH 7.5, 2 mM β-ME, 300 mM NaCl, 1 mM PMSF, 10% glycerol). Protein was eluted with Strep wash buffer containing 2.5 mM d-Desthiobiotin (Sigma, D1411) and stored at -80 °C after snap freezing in liquid nitrogen. The final construct contained a STREP tag at the C-terminus of MSH4 and a HIS-tag at the C-terminus of MSH5. The variants of the MSH4-MSH5 complex were purified using the same procedure. We note that the double mutant MSH4G685A-MSH5G597A heterodimer was not stable and could not be purified.

Purification of human EXO1(DA)

The pFB-EXO1(D173A)-FLAG vector was used to prepare recombinant baculovirus and the protein was expressed in *Sf*9 cells as described above. Frozen cell pellet was thawed and resuspended in 3 pellet volumes of lysis buffer [50 mM Tris-HCl pH 7.5, 0.5 mM β-ME, 1 mM EDTA, 1:400 (volume/volume) protease inhibitor cocktail (Sigma, P8340), 0.5 mM PMSF, 20 μg/ml leupeptin]. The cell suspension was incubated with gentle stirring for 10 min. 1/2 volume of 50% glycerol and 6.5% volume of 5 M NaCl (final concentration 305 mM) were added. The suspension was incubated for 30 min with stirring. The extract was then centrifuged at 48,000 x g for 30 min. The soluble extract was added to pre-equilibrated M2 anti FLAG affinity resin (Sigma, A2220, 2 ml resin for purification from 1 l *Sf*9 cell culture) and incubated batchwise for 45 min. The suspension was then centrifuged (2,000 x g, 5 min), the supernatant (FLAG flowthrough) removed, and the resin was transferred to a disposable chromatography column. The resin was washed with 50 resin volumes of TBS buffer (20 mM Tris-HCl pH 7.5, 150 mM NaCl, 0.5 mM β-ME, 0.5 mM PMSF, 10% glycerol) supplemented with 0.1% NP40. This was

followed by washing with 10 resin volumes of TBS buffer without NP40. EXO1-FLAG was eluted with TBS buffer supplemented with 150 ng/µl 3x FLAG peptide (Sigma, F4799). Fractions containing detectable protein (as estimated by the Bradford method) were pooled, applied on a disposable column with 1 ml pre-equilibrated Biorex70 resin (Bio-Rad), and flow-through was collected. The sample was then diluted by adding 1 volume of dilution buffer (50 mM Tris-HCl pH 7.5, 5 mM β-ME, 0.5 mM PMSF, 10% glycerol). Diluted FLAG-EXO1 was applied on 1 ml HiTrap SP HP column (GE Healthcare) pre-equilibrated with S buffer A (50 mM Tris-HCl pH 7.5, 75 mM NaCl, 5 mM β-ME, 10% glycerol) at 0.8 ml/min. The column was washed with 20 ml S buffer A, and eluted with 8 ml linear salt gradient in S buffer A (75 mM to 1 M NaCl). Peak fractions were pooled, aliquoted, frozen in liquid nitrogen and stored at -80 °C. The procedure yielded around ~0.15 mg of protein from 1 l of *Sf*9 culture, with an approximate concentration of ~1 µM.

Purification of human MSH2-MSH6 and MSH2-MSH3 heterodimers

To prepare the MSH2-MSH6 heterodimer, the *Sf*9 cells were co-infected with recombinant baculoviruses prepared from pFB-hMSH2-FLAG and pFB-hMSH6-HIS[33] vectors. The purification was carried out at 4 °C or on ice. The cell pellets were resuspended in 3 volumes of lysis buffer [50 mM Tris-HCl pH 7.5, 1:400 [volume/volume] protease inhibitor cocktail (Sigma, P8340), 1 mM PMSF, 60 µg/ml leupeptin, 0.5 mM β-ME, 20 mM imidazole]. The sample was incubated while stirring for 20 min. 1/2 volume of 50% glycerol was added, followed by 6.5% volume 5 M NaCl (final concentration 305 mM). The cell suspension was incubated for 30 min with stirring. To obtain soluble extract, the suspension was centrifuged (30 min, 48,000 x g). The supernatant was mixed with pre-equilibrated 2 ml NiNTA resin (purification from 800 ml *Sf*9 cells) and incubated batchwise for 1 h. The resin was then washed batchwise and on column with wash buffer [30 mM Tris-HCl pH 7.5, 1:1,000 (volume/volume) protease inhibitor cocktail (Sigma, P8340), 15 µg/ml leupeptin, 0.5 mM β-ME, 0.5 mM PMSF, 20 mM imidazole, 300 mM NaCl, 10% glycerol]. Bound protein was eluted with elution buffer [30 mM Tris-HCl pH 7.5, 1:1,000 (volume/volume) protease inhibitor cocktail (Sigma, P8340), 15 µg/ml leupeptin, 0.5 mM β-ME, 0.5 mM PMSF, 300 mM imidazole, 150 mM NaCl,

10% glycerol]. The pooled fractions were diluted with 7 volumes of dilution buffer (30 mM Tris-HCl pH 7.5, 15 µg/ml leupeptin, 0.5 mM β-ME, 0.5 mM PMSF, 150 mM NaCl, 10% glycerol), and mixed with 0.7 ml pre-equilibrated anti-FLAG M2 affinity gel (Sigma). The suspension was incubated batchwise for 60 min. The sample was centrifuged (5 min, 1,000 g) and resin was transferred to a disposable chromatography column. The resin was then washed extensively with dilution buffer. The heterodimer was eluted with dilution buffer supplemented with 200 µg/ml 3x FLAG peptide (Sigma). Eluates containing protein were pooled, aliquoted, frozen in liquid nitrogen and stored at -80 °C. The MSH2-MSH3 heterodimer was prepared using the same procedure, using pFB-hMSH3-HIS[35].

Purification of yeast Msh4-Msh5

Baculoviruses expressing Msh4 and Msh5 were prepared individually using the Bac-to-Bac system and pFB-yMSH4-STREP and pFB-yMSH5-HIS vectors. *Sf*9 cells were co-infected with optimized ratios of both viruses to express both proteins together as a heterodimer. The cells were harvested 52 h after infection, washed with PBS, and the pellets were frozen in liquid nitrogen and stored at -80 °C until use. The subsequent steps were carried out on ice or at 4 °C. The cell pellet was resuspended in lysis buffer [50 mM Tris-HCl pH 7.5, 2 mM β-ME, 1 mM EDTA, 1:400 (volume/volume) protease inhibitor cocktail (Sigma, P8340), 1 mM PMSF, 30 µg/ml leupeptin, 20 mM imidazole] for 20 min. Then, 50% glycerol was added to a final concentration of 16%, followed by 5 M NaCl to a final concentration of 305 mM. The suspension was incubated for further 30 min with gentle agitation. The total cell extract was centrifuged at 48,000 x g for 30 min to obtain soluble extract. The extract was then bound to NiNTA resin (Qiagen) for 60 min batchwise followed by extensive washing with NiNTA wash buffer (50 mM Tris-HCl pH 7.5, 2 mM β-ME, 300 mM NaCl, 10 % glycerol, 1 mM PMSF, 10 µg/ml leupeptin, 20 mM imidazole) both batchwise and on a column. The heterodimer was eluted by NiNTA elution buffer (NiNTA wash buffer containing 250 mM imidazole). The eluate was further incubated with pre-equilibrated Strep-Tactin Superflow resin (Qiagen) for 60 min batchwise. The protein-bound resin was then washed in two sequential steps; first with STREP wash buffer I (50 mM Tris pH 7.5, 2 mM β-ME, 10 % glycerol, 1 mM PMSF and 300 mM NaCl) and then with STREP wash buffer II

(50 mM Tris pH 7.5, 2 mM β-ME, 10 % glycerol, 1 mM PMSF and 50 mM NaCl). The heterodimer was eluted with STREP wash buffer II containing 2.5 mM d-Desthiobiotin (Sigma). The eluate was then applied on a pre-equilibrated HiTrap Q HP column (GE Healthcare). The column was washed with STREP wash buffer II and protein was eluted with a linear gradient of NaCl (50 to 600 mM) in STREP wash buffer II. Collected fractions were analyzed on SDS-PAGE, peak samples were pooled, aliquoted and stored at -80 °C. The final construct contained a STREP tag at the C-terminus of yMsh4 and a HIS-tag at the C-terminus of yMsh5. The procedure yielded ~ 0.15 mg of protein from 4 l of *Sf*9 culture, with an approximate concentration of ~ 1 μM.

Purification of yeast Mlh1-Mlh3

The yMlh1-yMlh3 heterodimer was expressed using pFB-HIS-yMLH1 and pFB-MBP-yMLH3 and the Bac-to-Bac system and purified using affinity chromatography[11]. Briefly, the cells were resuspended in lysis buffer containing 50 mM Tris-HCl pH 7.5, 1 mM DTT, 1 mM EDTA, 1:400 (volume/volume), protease inhibitor cocktail (Sigma, P8340), 1 mM PMSF, 30 μg/ml leupeptin and incubated for 20 min. Subsequently glycerol [final concentration 16% (volume/volume)] and NaCl (final concentration 305 mM) were added. Upon further incubation for 30 min and centrifugation (48,000 x g, 30 min), the cleared extract was then subjected to affinity chromatography with Amylose resin (New England Biolabs), the MBP tag was cleaved with PreScission protease and the heterodimer was further purified on Ni-NTA agarose (Qiagen)[11]. The final eluate was dialyzed into 50 mM Tris-HCl pH 7.5, 5 mM β-ME, 10% glycerol, 0.5 mM PMSF and 300 mM NaCl. Aliquots were flash frozen and stored at -80 °C until use. The purification yielded ~ 1 mg protein from 2.4 l culture and the concentration was 5.9 μM.

Purification of yeast and human RFC, PCNA and the Ku heterodimer

Human PCNA was expressed in *E. coli* cells (1 l) from pET23C-his-hPCNA vector (a kind gift from Ulrich Huebscher, University of Zurich). Transformed cells were grown to OD 0.5, and induced with 0.5 mM isopropyl β-D-1-thiogalactopyranoside (IPTG) for 3.5 h at 37 °C. Cells were lysed by sonication in lysis buffer (20

687 mM Tris-HCl pH 7.5, 250 mM NaCl, 2 mM β-ME, 5 mM imidazole, 1 mM PMSF,
688 1:250 Sigma protease inhibitor cocktail P8340). The lysate was cleared by cen-
689 trifugation (48,000 x g, 30 min) and bound to 2 ml NiNTA resin (Qiagen) for 1 h
690 batchwise. Resin was washed with wash buffer (20 mM Tris-HCl pH 7.5, 250 mM
691 NaCl, 2 mM β-ME, 30 mM imidazole, 1 mM PMSF), and PCNA was eluted with elu-
692 tion buffer (wash buffer supplemented with 400 mM imidazole). The sample was
693 diluted to conductivity corresponding to 100 mM NaCl, and loaded on HiTrap Q
694 column. The column was developed by a salt gradient (100 mM to 1 M NaCl) in 20
695 mM Tris-HCl pH 7.5, 2 mM β-ME and 10% glycerol. The fractions containing PCNA
696 were pooled, aliquoted and stored at -80 °C. Yeast PCNA was prepared as de-
697 scribed[36].

698 To express human RFC, the *Sf*9 cells (1.4 l) were infected with recombinant
699 baculovirus prepared with vector pFBDM-MBP-RFC1-RFC2-3-4-His-5 (a kind
700 gift from Josef Jiricny, ETH Zurich, RFC1 subunit MBP-tagged and RFC5 subunit
701 his-tagged). The purification was carried out at 4 °C or on ice. The cell pellets
702 were resuspended in 3 volumes lysis buffer [50 mM Tris-HCl pH 7.5, 2 mM β-ME,
703 1:300 (volume/volume) protease inhibitor cocktail (Sigma, P8340), 1 mM PMSF,
704 30 μg/ml leupeptin, 15 mM imidazole). The cells were let swelling on ice for 20
705 min and mixed occasionally. Afterwards, 1/2 volume of 50% glycerol was added,
706 followed by 6.5% volume 5 M NaCl (final concentration 305 mM), and the sus-
707 pension was incubated while stirring for 30 min. The cell suspension was centri-
708 fuged at 55,000 x g for 30 min to obtain soluble extract. The supernatant was
709 mixed with pre-equilibrated 2 ml NiNTA resin (Qiagen) and batch incubated with
710 gentle agitation for 1 h. The resin was washed 3 times batchwise, and with 15
711 resin volumes on column with wash buffer I (50 mM Tris-HCl pH 7.5, 2 mM β-ME,
712 0.25 M NaCl, 10% Glycerol, 1 mM PMSF, 20 mM imidazole). The RFC complex was
713 eluted with NiNTA elution buffer (50 mM Tris-HCl pH 7.5, 2 mM β-ME, 250 mM
714 NaCl, 10% glycerol, 1 mM PMSF, 300 mM imidazole). The eluate was directly ap-
715 plied in flow on 1.5 ml amylose resin (New England Biolabs) pre-equilibrated
716 with wash buffer 2 (50 mM Tris pH 7.5, 2 mM β-ME, 0.1 M NaCl, 10% Glycerol, 1
717 mM PMSF), and washed with wash buffer 2. The RFC complex was eluted with
718 wash buffer 2 supplemented with 10 mM maltose. The protein concentration was
719 estimated by the Bradford method, and the sample was incubated with 20%

(w/w) Prescission protease for 2 h at 4 °C. The sample was then applied on HiTrap Q column (0.5 ml/min), pre-equilibrated in Q buffer A (50 mM Tris pH 7.5, 5 mM β-ME, 0.1 M NaCl, 10% Glycerol), the column was then washed with Q buffer A, and eluted in the same buffer with a salt gradient (0.1 M to 1 M) in 6 column volumes. The fractions containing RFC were pooled, aliquoted, frozen in liquid nitrogen and stored at -80 °C. The purification yielded ~ 1 ml of 8.5 μM RFC.

Yeast RFC was expressed in *E. coli* cells (4 l) transformed with pEAO271 (a kind gift from E. Alani, Cornell University). Cells were grown to OD 0.5, and induced with 0.5 mM IPTG for 3 h at 37 °C. Cells were resuspended in lysis buffer (60 mM HEPES-NaOH pH 7.5, 250 mM NaCl, 2 mM β-ME, 0.5 mM EDTA, 1:250 Sigma protease inhibitor cocktail P8340, 1 mM PMSF, 10% glycerol) and disrupted by sonication. The cleared extract was loaded on 5 ml HiTrap SP column, washed with buffer SP A (30 mM HEPES-NaOH pH 7.5, 300 mM NaCl, 2 mM β-ME, 0.5 mM EDTA, 1 mM PMSF, 10% glycerol) and eluted with a salt gradient (300 mM to 600 mM NaCl). Eluted fractions were analyzed by polyacrylamide gel electrophoresis, pooled and diluted to conductivity corresponding to 110 mM NaCl. The diluted sample was applied on HiTrap Q column, and eluted in 110 to 600 mM NaCl gradient in 30 mM HEPES-NaOH pH 7.5, 2 mM β-ME, 1 mM PMSF and 10% glycerol. The eluate was aliquoted and stored at -80 °C. The preparation of the yeast Ku heterodimer was described previously[37].

Nuclease assays

The reactions (15 μl) were carried out in 25 mM Tris-acetate pH 7.5, 1 mM DTT, 0.1 mg/ml bovine serum albumin (BSA, New England Biolabs), and as indicated manganese or magnesium acetate (5 mM), ATP (concentrations as indicated, GE Healthcare, 27-1006-01) and plasmid-based DNA substrate [100 ng per reaction, either 2.7 kbp-long pUC19 (Fig. 1 and related Extended Data Figures), 5.6 kbp-long pFB-RPA2 (Figures 2 and 3, and related Extended Data Figures), 10.3 kbp-long pFB-HIS-MBP-hMLH3co (Extended Data Fig. 4j), or pAG25 (Addgene) or cruciform pIRbke8 mut[25] (Fig. 2f, Extended Data Fig. 4k)]. In experiments with ^{32}P-labeled oligonucleotide-based DNA the substrate concentration was 1 nM, in

752 molecules. Where indicated, ADP (Alfa Aesar, J60672), AMP-PNP (Toronto Chem-
753 ical, A634303) or ATP-γ-S (Cayman, 14957) were used instead of ATP. Where in-
754 dicated, the reactions were supplemented with PIP box peptide derived from p21
755 (GRKRRQTSMTDFYHSKRRLIFS) or control peptide with key residues mutated
756 (underlined, GRKRRATSATDFYHSKRRLIFS)(Genecust). The reaction buffer was
757 assembled on ice, and the recombinant proteins were then added on ice (MLH1-
758 MLH3 protein was always added last). The reactions, unless indicated otherwise,
759 were incubated for 60 min at 30 °C or 37 °C. The reactions were supplemented
760 with protein storage or dilution buffer to compensate for components introduced
761 with recombinant proteins in each particular experiment, this resulted in final
762 NaCl concentrations ~30 mM. The reactions were terminated with 5 µl STOP so-
763 lution (150 mM EDTA, 2% SDS, 30% glycerol, 0.01% bromophenol blue), 1 µl pro-
764 teinase K (Roche, 03115828001, 18 mg/ml) and further incubated for 60 min at
765 50 °C. The reaction products were then separated by electrophoresis in 1% aga-
766 rose (Sigma, A9539) containing GelRed (Biotium) in TAE buffer. Using Bio-Rad
767 SubCell GT system (gel length 26 cm), the separation was carried out for 90 min
768 at 120 V. The gels were then imaged (InGenius3, GeneSys). The results were quan-
769 titated using ImageJ and expressed as % of nicked DNA versus the total DNA in
770 each particular lane; any nicked DNA present in control (no protein) reactions
771 was removed as a background. For gel source data, see Supplementary Figure 1.
772
773 **Electrophoretic mobility shift assays**
774 The DNA binding reactions were carried out in 15 µl volume in binding buffer
775 containing 25 mM HEPES pH 7.8, 5 mM magnesium chloride, 5% (volume/vol-
776 ume) glycerol, 1 mM DTT, 50 µg/ml BSA, 6.6 ng/µl dsDNA (in assays with yeast
777 proteins) or 3.3 ng/µl dsDNA (in assays with human proteins) as competitor (50
778 bp-long), 0.5 nM DNA substrate (^{32}P-labelled, in molecules) and respective con-
779 centrations of recombinant proteins (yeast or human MSH4-MSH5 complex and
780 their variants, MLH1-MLH3 and variants). The oligonucleotide-based DNA sub-
781 strates were ssDNA (labelled oligonucleotide PC1253), dsDNA (labelled PC1253
782 and PC1253C), Y-structure (labelled PC1254 and PC1253), HJ (labelled PC1253
783 and PC1254, PC1255 and PC1256) and D-Loop (labelled BB, and BT, INVa and
784 INVb). $MgCl_2$ was replaced by 3 mM EDTA where indicated. The reactions were

assembled and incubated on ice for 15 min, followed by the addition of 5 µl EMSA loading dye (50% glycerol, 0.01% bromophenol blue). The products were separated on 6% native polyacrylamide gel (19:1 acrylamide-bisacrylamide, BioRad) on ice. The gels were dried on 17 CHR paper (Whatman), exposed to storage phosphor screens (GE Healthcare), and scanned by Phosphorimager (Typhoon FLA 9500, GE Healthcare). The quantitation was carried out by ImageQuant software (GE Healthcare) and graphs were plotted using Prism software (Prism 8, Graphpad). For gel source data, see Supplementary Figure 1.

For the "super-shift" assays comprising yMlh1-yMlh3 and yMsh4-yMsh5, the reactions were carried out as mentioned above (with magnesium or EDTA, as indicated), except that the products were separated on 0.6% agarose gel in TAE buffer at 4 °C (1 h, 100 V). The gels were dried on DE81 paper (Whatman) and scanned as above. In the super-shift assays with MLH1-MLH3, MSH4-MSH5 and EXO1, the reaction buffer additionally contained 75 mM NaCl and 10 µM ATP. The DNA binding assays with yKu70-80 were carried out similarly, without salt and ATP, and were incubated for 30 min at 30 °C.

Protein interaction assays

To test for protein-protein interactions, recombinant “bait” protein was immobilized on beads coupled to a specific antibody and incubated with the “prey” protein. After removal of unbound protein by beads washing, proteins were either detected by silver staining or by western blot. For gel source data, see Supplementary Figure 1.

To test for the interaction between MLH1-MLH3 and MSH4-MSH5, 0.7 µg anti-MLH1 antibody (Abcam, ab92312) was captured on 15 µl Protein G magnetic beads (Dynabeads, Invitrogen) by incubating in 50 µl PBS-T (PBS with 0.02% Tween-20) for 60 min with gentle mixing at regular intervals. The beads were washed 3 times on magnetic racks with 150 µl PBS-T to remove unbound antibodies. The beads were then mixed with 165 nM recombinant MLH1-MLH3 and 220 nM MSH4-MSH5 in 50 µl binding buffer I (25 mM HEPES pH 7.8, 3 mM EDTA, 1 mM DTT, 50 µg/ml BSA, 80 mM NaCl) and incubated on ice for 45 min with gentle agitation at regular intervals. Beads were then washed 3 times with 150 µl

wash buffer I (25 mM HEPES pH 7.8, 3 mM EDTA, 1 mM DTT, 0.02% Tween-20, 80 mM NaCl) and proteins were eluted by boiling the beads in SDS buffer (50 mM Tris-HCl pH 6.8, 1.6% sodium dodecyl sulphate, 100 mM DTT, 10% glycerol, 0.01% bromophenol blue) for 3 min at 95 °C. The eluate was separated on a 10% SDS-PAGE gel and proteins were detected by silver staining. To perform the experiment reciprocally, 5 μg anti-HIS antibody (Genscript, A00186) was captured on Protein G beads (Dynabeads, Invitrogen) as described above. The recombinant protein complexes, as above, were then added and incubated in 50 μl binding buffer II (25 mM HEPES pH 7.8, 3 mM EDTA, 1 mM DTT, 50 μg/ml BSA, 80 mM NaCl) for 45 min with gentle agitation at regular intervals. Beads were then washed 3 times with wash buffer II (25 mM HEPES pH 7.8, 3 mM EDTA, 1 mM DTT, 80 mM NaCl, 0.1% Triton X-100). The subsequent steps were carried out as described above. To test for species-specific interactions as shown in Extended Data Fig. 3g, the same procedure was followed except 100 nM of either human MSH4-MSH5 or yeast Msh4-Msh5 was incubated with 400 nM MLH1-MLH3. To test for the interaction between yeast Mlh1-Mlh3 and Msh4-Msh5, 10 μl Protein G beads were used to capture 1 μg anti-STREP antibody (Biorad, MCA2489). yMsh4-yMsh5 (120 nM) was incubated with the beads in 60 μl binding buffer III (25 mM Tris-HCl pH 7.5, 3 mM EDTA, 1 mM DTT, 20 mg/ml BSA, 60 mM NaCl) for 60 min with continuous mixing. Next, the beads were washed 3 times with 150 μl wash buffer III (25 mM Tris-HCl pH 7.5, 3 mM EDTA, 1 mM DTT, 120 mM NaCl, 0.05% Triton X-100). 300 nM yMlh1-yMlh3 was then added to the resuspended beads in 60 μl binding buffer III, and incubated for additional 60 min with continuous mixing. Beads were washed 3 times with 150 μl wash buffer III and boiled afterwards for 3 min at 95 °C in SDS buffer to elute the proteins. The protein complexes were detected by western blot with anti-HIS antibody (Genscript, A00186).

To test for the interaction between MLH1-MLH3 and EXO1, 0.33 μg anti-MLH1 antibody (Abcam ab223844) was captured on 10 μl protein G magnetic beads (Dynabeads, Invitrogen) by incubating in 50 μl PBS-T (PBS with 0.1% Tween-20) for 2 h at 4 °C with gentle mixing at regular intervals. The beads were washed 4 times on magnetic racks with 150 μl PBS-T to remove unbound antibody. The beads were then mixed with 1 μg recombinant MLH1-MLH3 and 0.5 μg EXO1 in

200 µl binding buffer I (25 mM Tris-HCl pH 7.5, 3 mM EDTA, 1 mM DTT, 20 µg/ml BSA, 300 mM NaCl) and incubated on ice for 2 h with gentle agitation at regular intervals. Beads were then washed 4 times with 300 µl wash buffer I (50 mM Tris-HCl pH 7.5, 3 mM EDTA, 1 mM DTT, 300 mM NaCl, 0.05% Triton X-100) and proteins were eluted by boiling the beads in SDS buffer (50 mM Tris-HCl pH 6.8, 1.6% sodium dodecyl sulphate, 100 mM DTT, 10% glycerol, 0.01% bromophenol blue) for 3 min at 95 °C. The eluate was separated on a 10% SDS-PAGE gel and proteins were detected by silver staining.

To test for the interaction between human MLH1-MLH3 and human PCNA or EXO1, 1 µg anti-MLH1 antibody (Abcam ab223844) was captured on 15 µl protein G magnetic beads (Dynabeads, Invitrogen) by incubating in 50 µl PBS-T (PBS with 0.1% Tween-20) for 1 h at room temperature with gentle mixing at regular intervals. The beads were washed 3 times on magnetic racks with 150 µl PBS-T to remove unbound antibody. The beads were then mixed with 1.5 µg each recombinant MLH1-MLH3 and PCNA or EXO1, in 60 µl binding buffer I (25 mM Tris-HCl pH 7.5, 3 mM EDTA, 1 mM DTT, 20 µg/ml BSA, 60 mM NaCl) and incubated on ice for 1 h with gentle agitation at regular intervals. Beads were then washed 4 times with 150 µl wash buffer I (50 mM Tris-HCl pH 7.5, 3 mM EDTA, 1 mM DTT, 120 mM NaCl, 0.05% Triton X-100) and proteins were eluted by boiling the beads in SDS buffer (50 mM Tris-HCl pH 6.8, 1.6% sodium dodecyl sulphate, 100 mM DTT, 10% glycerol, 0.01% bromophenol blue) for 3 min at 95 °C. Avidin (Sigma, A9275, 110 ng/µl) was added to the eluate as a stabilizer. The eluate was separated on a 10% SDS-PAGE gel and proteins were detected by silver staining.

Yeast manipulations

All yeast strains are derivatives of the SK1 background and are listed in Supplementary Data Table 2. Yeast strains were obtained by direct transformation or crossing to obtain the desired genotype. The following alleles have been described previously: *mlh1Δ*, *mlh3Δ* as well as spore-autonomous fluorescent marker for the live cell recombination assays[38,39].

YIplac211 plasmid derivatives carrying *MLH1* (pYIplac211-*MLH1*, pML535) or *MLH3* (pYIplac211-*MLH3*, pML536), as well as the respective promoter (~ 500 bp

upstream of ATG) and terminator (~ 200 bp downstream of STOP) regions were used to complement *mlh1Δ* or *mlh3Δ* mutant strains, respectively. pYIplac211-*MLH1* and pYIplac211-*MLH3* were linearized and integrated in the promoter region of the respective genomic loci. pYIplac211-*MLH1*$^{Q572A\text{-}L575A\text{-}F578A}$ (pML538), encoding Mlh1^{P}, and pYIplac211-*MLH3*$^{Q293A\text{-}V296A\text{-}F300A}$ (pML540), encoding Mlh3^{P}, were generated by restriction digest-mediated insertion of a synthetic fragment carrying the respective mutations into pYIplac211-*MLH1* or pYIplac211-*MLH3*. PCR-based C-terminal tagging of *MLH1* and *MLH3* was performed using standard procedures[40].

Rfc1 was C-terminally tagged with TAP tag. The Mlh1-HA and the internally FLAG-Myc-tagged Mlh3 constructs were described previously[30,41]. Transformants were confirmed using PCR discriminating between correct and incorrect integrations and sequencing. All experiments were performed at 30 °C. Two different approaches were used for meiosis induction. In the first one, cells were grown in SPS presporulation medium and transferred in sporulation medium as described[42]. For highly synchronous copper-inducible meiosis, the procedure was described[43]. Briefly, cells were grown in YPD to exponential phase. Exponentially growing yeast were inoculated at OD_{600} = 0.05 into reduced glucose YPD (1% yeast extract, 2% peptone, 1% glucose) and grown to an OD_{600} = 11-12 for 16-18 h. Cells were washed, resuspended in sporulation medium (1.0% [w/v] potassium acetate, 0.02% [w/v] raffinose, 0.001% polypropylene glycol) at OD_{600} = 2.5. After 2 h, copper(II) sulfate (50 µM) was added to induce *IME1* expression from the *CUP1* promoter.

Analysis of recombination using spore-autonomous fluorescence

The spore-autonomous fluorescence analysis of recombination was performed as described[39], with minor modifications. Diploid yeast cell colonies were streaked on $YP_{2\%glycerol}$ plates, grown for 48 h, and single colonies were expanded twice in YPD plates at 30 °C for 24 h. Cells were then transferred to sporulation medium plates (SPM, 2% KAc) and incubated at 30 °C for 48 h. Spores were resuspended in SPM, briefly sonicated and transferred onto Poly-L-Lysine coated microscopy slides. Images were captured in four channels using a Wide-field DeltaVision multiplexed microscope with a 60x 1.4NA DIC Oil PlanApoN objective and a peco.edge

5.5 camera under the control of Softworx (Applied Precision). Images were processed in Fiji and the pattern of spore fluorescence in tetrads was manually scored. Only tetrads with each fluorescent marker occurring in two spores were included in the final assay. Recombination frequency, expressed as map distance in centimorgans was calculated using the Stahl lab online tools (https://elizabethhousworth.com/StahlLabOnlineTools/)[44]. Three replicates using independent clones were analyzed. ≥900 tetrads were scored for each genotype.

Analysis of spore viability

Spore viability was determined by microdissection of ≥ 156 spores from at least two independent experiments after induction of meiosis on SPM plates at 30 °C for 24 h.

Protein stability analyses by western blotting

Protein extracts from yeast were performed using the trichloroacetic acid (TCA) method[45]. Briefly, exponentially growing cultures were harvested and disrupted using glass beads in 10% TCA. Precipitates were collected by centrifugation, resuspended in 2x NuPAGE sample buffer (Invitrogen), and neutralized with 1 M Tris. Samples were then boiled at 95 °C for 5 min, cleared by centrifugation, and separated in NuPAGE 3-8% Tris-Acetate gels (Invitrogen). After gel electrophoresis, proteins were transferred onto PVDF membranes (GE Healthcare). Antibodies targeting the following tags or proteins were used: mouse anti-FLAG HRP-conjugated (1:15,000, A8592-1MG, Sigma), rabbit anti-FLAG (1:2000, F7425-.2MG Sigma), rabbit anti-Crm1 (1:5000, a gift from K. Weis, ETH Zurich), swine anti-rabbit HRP-conjugated (1:5000, P0399, Dako). For gel source data, see Supplementary Figure 1.

Co-immunoprecipitation and Western blot analysis

$1.2x10^9$ cells were harvested, washed once with PBS, and lysed in 3 ml lysis buffer [20 mM HEPES-KOH pH 7.5, 150 mM NaCl, 0.5% Triton X-100, 10% glycerol, 1 mM $MgCl_2$, 2 mM EDTA; 1 mM PMSF; 1 x Complete Mini EDTA-Free (Roche); 1X PhosSTOP (Roche); 125 U/ml benzonase] with glass beads three times for 30 s in a Fastprep instrument (MP Biomedicals, Santa Ana, CA). The lysate was incubated

1 h at 4 °C. 100 µl of PanMouse IgG magnetic beads (Thermo Scientific) were washed with 100 µl lysis buffer, preincubated in 100 µg/ml BSA in lysis buffer for 2 h at 4 °C and then washed twice with 100 µl lysis buffer. The lysate was cleared by centrifugation at 13,000 x g for 5 min and incubated overnight at 4 °C with washed PanMouse IgG magnetic beads. The magnetic beads were washed four times with 1 ml wash buffer [20 mM HEPES-KOH pH7.5, 150 mM NaCl, 0.5% Triton X-100, 5% Glycerol, 1 mM $MgCl_2$, 2 mM EDTA, 1 mM PMSF, 1 x Complete Mini EDTA-Free (Roche)]. The beads were resuspended in 30 µl TEV-C buffer (20 mM Tris-HCl pH 8, 0.5 mM EDTA, 150 mM NaCl, 0.1% NP-40, 5% glycerol, 1 mM MgCl2, 1 mM DTT) with 3 µl TEV protease (1 mg/ml) and incubated for 2 h at 23 °C under agitation. The eluate was transferred to a new tube. Beads eluate was heated at 95 °C for 10 min and loaded on polyacrylamide gel [4-12% Bis-Tris gel (Invitrogen)] and run in MOPS SDS Running Buffer (Life Technologies). Proteins were then transferred to PVDF membrane using Trans-Blot® Turbo™ Transfer System (Biorad) at 1 A constant, up to 25 V for 45 min. Proteins were detected using c-Myc mouse monoclonal antibody (9E10, Santa Cruz, 1:500), HA.11 mouse monoclonal antibody (16B12, Biolegend, 1:750) or TAP rabbit monoclonal antibody (Invitrogen, CAB1001, 1:4,000). The TAP antibody still detects the CBP (Calmodulin Binding Protein) moiety after TEV cleavage of the TAP tag. Signal was detected using the SuperSignal West Pico or Femto Chemiluminescent Substrate (ThermoFisher). Images were acquired with a Chemidoc system (Biorad). For gel source data, see Supplementary Figure 1.

Chromatin immunoprecipitation and real-time quantitative PCR

For each meiotic time point, $2x10^8$ cells were processed as described[46], with the following modifications: lysis was performed in lysis buffer plus 1 mM PMSF, 50 µg/ml aprotinin and 1x Complete Mini EDTA-Free (Roche), using 0.5 mm zirconium/silica beads (Biospec Products, Bartlesville, OK). The lysate was directly applied on 50 µl PanMouse IgG magnetic beads. Before use, magnetic beads were blocked with 5 µg/µl BSA for 4 h at 4 °C.

Quantitative PCR was performed from the immunoprecipitated DNA or the whole cell extract using a QuantStudio 5 Real-Time PCR System and SYBR Green PCR master mix (Applied Biosystems, Thermo Scientific) as described[46]. Results were

expressed as % of DNA in the total input present in the immunoprecipitated sample and normalized by the negative control site in the middle of *NFT1*, a 3.5 kb long gene. For the meiotic time-course in Figure 3f, the data were further normalized by the value at the 2 h time-point (time of meiosis induction by copper addition). Primers for *GAT1*, *BUD23*, *HIS4LEU2*, Axis and *NFT1* have been described[30].

ADDITIONAL REFERENCES

31 El-Shemerly, M., Hess, D., Pyakurel, A. K., Moselhy, S. & Ferrari, S. ATR-dependent pathways control hEXO1 stability in response to stalled forks. *Nucleic Acids Res* **36**, 511-519, doi:10.1093/nar/gkm1052 (2008).

32 Cannavo, E. & Cejka, P. Sae2 promotes dsDNA endonuclease activity within Mre11-Rad50-Xrs2 to resect DNA breaks. *Nature* **514**, 122-125, doi:10.1038/nature13771 (2014).

33 Iaccarino, I., Marra, G., Palombo, F. & Jiricny, J. hMSH2 and hMSH6 play distinct roles in mismatch binding and contribute differently to the ATPase activity of hMutSalpha. *EMBO J* **17**, 2677-2686, doi:10.1093/emboj/17.9.2677 (1998).

34 Anand, R., Pinto, C. & Cejka, P. Methods to Study DNA End Resection I: Recombinant Protein Purification. *Methods Enzymol* **600**, 25-66, doi:10.1016/bs.mie.2017.11.008 (2018).

35 Palombo, F. *et al.* hMutSbeta, a heterodimer of hMSH2 and hMSH3, binds to insertion/deletion loops in DNA. *Curr Biol* **6**, 1181-1184, doi:10.1016/s0960-9822(02)70685-4 (1996).

36 Biswas, E. E., Chen, P. H. & Biswas, S. B. Overexpression and rapid purification of biologically active yeast proliferating cell nuclear antigen. *Protein Expr Purif* **6**, 763-770, doi:10.1006/prep.1995.0007 (1995).

37 Reginato, G., Cannavo, E. & Cejka, P. Physiological protein blocks direct the Mre11-Rad50-Xrs2 and Sae2 nuclease complex to initiate DNA end resection. *Genes Dev*, doi:10.1101/gad.308254.117 (2018).

38 Arter, M. *et al.* Regulated Crossing-Over Requires Inactivation of Yen1/GEN1 Resolvase during Meiotic Prophase I. *Dev Cell* **45**, 785-800 e786, doi:10.1016/j.devcel.2018.05.020 (2018).

39 Thacker, D., Lam, I., Knop, M. & Keeney, S. Exploiting spore-autonomous fluorescent protein expression to quantify meiotic chromosome behaviors in Saccharomyces cerevisiae. *Genetics* **189**, 423-439, doi:10.1534/genetics.111.131326 (2011).

40 Wild, P. *et al.* Network Rewiring of Homologous Recombination Enzymes during Mitotic Proliferation and Meiosis. *Mol Cell* **75**, 859-874 e854, doi:10.1016/j.molcel.2019.06.022 (2019).

41 Duroc, Y. *et al.* Concerted action of the MutLbeta heterodimer and Mer3 helicase regulates the global extent of meiotic gene conversion. *Elife* **6**, doi:10.7554/eLife.21900 (2017).

42 Murakami, H., Borde, V., Nicolas, A. & Keeney, S. Gel electrophoresis assays for analyzing DNA double-strand breaks in Saccharomyces cerevisiae

at various spatial resolutions. *Methods Mol Biol* **557**, 117-142, doi:10.1007/978-1-59745-527-5_9 (2009).
43 Chia, M. & van Werven, F. J. Temporal Expression of a Master Regulator Drives Synchronous Sporulation in Budding Yeast. *G3 (Bethesda)* **6**, 3553-3560, doi:10.1534/g3.116.034983 (2016).
44 Stahl, F. W. & Lande, R. Estimating interference and linkage map distance from two-factor tetrad data. *Genetics* **139**, 1449-1454 (1995).
45 Matos, J. *et al.* Dbf4-dependent CDC7 kinase links DNA replication to the segregation of homologous chromosomes in meiosis I. *Cell* **135**, 662-678, doi:10.1016/j.cell.2008.10.026 (2008).
46 Borde, V. *et al.* Histone H3 lysine 4 trimethylation marks meiotic recombination initiation sites. *EMBO J* **28**, 99-111, doi:10.1038/emboj.2008.257 (2009).

MAIN TEXT STATEMENTS

Acknowledgements

This work was supported by grants from the Swiss National Science Foundation (31003A_17544) and ERC (681-630) to P.C., Institut Curie and CNRS to V.B., by Agence Nationale de la Recherche (ANR-15-CE11-0011) to V.B. and J.-B.C., by the Novo Nordisk Foundation (NNF15OC0016662) and ERC (724718) to E.R.H, and the Swiss National Science Foundation (155823 and 176108) to J.M. We thank Josef Jiricny (ETH Zurich) and members of the Cejka laboratory for helpful comments on the manuscript and Neil Hunter for communicating results prior to publication.

Conflict of interest

The authors declare no conflict of interest.

Author contributions

E.C., A.S., R.A. and P.C. planned, performed and analyzed the majority of the experiments and wrote the paper. L.R. and A.A. performed most of the experiments with yeast recombinant proteins and electrophoretic mobility shift assays. N.W. performed experiments to define simultaneous DNA binding by MLH1-MLH3 and MSH4-MSH5. J.H. performed experiments with yeast *mlh1* and *mlh3* variants mutated in PIP-box-like sequences, and the data were analyzed together with J.M. Chip experiments and Rfc1-Mlh1 and Rfc1-Mlh3 pulldown assays were carried

out by C.A., the data were analyzed together with V.B. J-B.C. helped prepare the MLH1-MLH3 expression construct and designed experiments with the PIP-box peptide. X.A-G. and E.R.H. prepared the MSH4-MSH5 expression construct. All authors contributed to prepare the final version of the manuscript.

Data Availability Statement

All relevant data generated or analyzed during this study are included in this published article and its supplementary information file.

EXTENDED DATA FIGURE LEGENDS

Extended Data Figure 1. ATP hydrolysis promotes MLH1-MLH3 to nick scDNA. a, A scheme of MLH1 and MLH3 constructs. The maltose-binding protein (MBP) on MLH3 was cleaved during protein purification. **b**, Recombinant MLH1-MLH3 used in this study. The 4-15% gradient polyacrylamide gel was stained with Coomassie Blue. **c**, Nuclease assay with MLH1-MLH3 and 2.7 kbp-long supercoiled DNA (scDNA) as a substrate. The reaction with 5 mM manganese acetate was incubated without ATP at 37 °C. **d**, Quantitation of assays such as in c. Averages shown; error bars, SEM; n=3. **e**, Nuclease assay with MLH1-MLH3 (300 nM) and 2.7 kbp-long scDNA. Linear DNA was used as a marker. The assay was carried out at 37 °C and contained 5 mM manganese acetate and ATP (0.5 mM). The MLH1-MLH3 nuclease introduces nicks in dsDNA but does not linearize dsDNA. **f**, Quantitation of nuclease assays with MLH1-MLH3 without or with ATP (0.5 mM), in the presence of manganese (5 mM). Averages shown; error bars, SEM; n=4. **g**, Nuclease assay with MLH1-MLH3 and 5 mM magnesium acetate. The reaction buffer contained ATP (0.5 mM). The assay was carried out at 37 °C. The heterodimer exhibits barely detectable nuclease activity in magnesium. **h**, Nuclease assay with MLH1-MLH3 and various nucleotide cofactors (ADP, ATP and non-hydrolysable ATP analogs ATP-γ-S and AMP-PNP, all 0.5 mM). The assay was carried out at 37 °C with 5 mM manganese acetate. The panel shows a representative experiment. **i**, Quantitation of nuclease assays such as in panel h, supplemented with various nucleotide co-factors and their analogs (0.5 mM). Averages shown; error bars,

SEM; n=4. **j**, Purified MLH1-MLH3 variants used in this study. MLH1(EA), MLH1(E34A); MLH3(EA), MLH3(E28A); MLH3(3ND), MLH3(D1223N-Q1224K-E1229K). The 4-15% gradient polyacrylamide gel was stained with Coomassie Blue. **k**, Alignment of MLH1 and MLH3 ATPase motifs. Conserved residues are highlighted in red. Alanine substitutions in MLH3 and MLH1 mutants used in this study are in italics. **l**, Nuclease assay with wild type MLH1-MLH3 and indicated variants deficient in ATP hydrolysis, without or with ATP (0.5 mM). The assay was carried out at 37 °C, with 5 mM manganese acetate. The panel shows a representative experiment. **m**, Quantitation of nuclease assays as shown in panel l, without or with ATP (0.5 mM), with either wild type or MLH1-MLH3 variants mutated in conserved ATPase domain residues. Averages shown; error bars, SEM; n≥4. **n**, Electrophoretic mobility shift assay with indicated MLH1-MLH3 variants, oligonucleotide-based HJ as the substrate, in the absence of ATP and no magnesium (with 3 mM EDTA). Asterisk (*) indicates the position of the radioactive label. A representative experiment is shown at the bottom, a quantitation (averages shown, n=3; error bars, SEM) at the top. **o**, Nuclease assays with wild type MLH1-MLH3 on oligonucleotide-based DNA substrates (Holliday junction, HJ and nicked Holliday junction, nicked HJ). The asterisk indicates the position of the radioactive label. The assay was carried out at 37 °C, with 5 mM manganese or magnesium acetate, as indicated, with ATP (1 mM). The products were analyzed by 10% native polyacrylamide gel electrophoresis.

Extended Data Figure 2. Human and yeast MutSγ complexes preferentially bind branched DNA intermediates. a, Recombinant human MSH4-MSH5 used in this study. **b**, Electrophoretic mobility shift assays with human MSH4-MSH5 and indicated DNA substrates. Asterisk (*) indicates the position of the radioactive label. The assays were carried out in a buffer containing 2 mM magnesium acetate without ATP. **c**, Quantitation of DNA binding assays such as shown in panel b. Averages shown; error bars, SEM; n=3. **d**, Electrophoretic mobility shift assays with yeast Msh4-Msh5 and indicated DNA substrates. Asterisk (*) indicates the position of the radioactive label. The assays were carried out in a buffer containing 2 mM magnesium acetate without ATP. **e**, Quantitation of experiments such as shown in panel d. Averages shown; error bars, range; n=2. **f**,

Quantification of electrophoretic mobility shift assays with yeast Msh4-Msh5 and indicated DNA substrates, without magnesium (with 3 mM EDTA). Averages shown; error bars, range; n=2.

Extended Data Figure 3. MutSγ and MutLγ physically interact and moderately stabilize each other at DNA junctions. a, To investigate the interplay of MutLγ and MutSγ at DNA junctions, we performed electrophoretic mobility shift assays with either or both complexes under more stringent conditions (75 mM NaCl, 2 mM magnesium acetate), separated on 0.6% agarose gels. Under these conditions, MSH4-MSH5 lost the capacity to stably bind HJs/D-Loops, but could help stabilize the MutSγ-MutLγ complex. The binding of MutLγ alone was not stable, as evidenced by a weak protein-DNA band and the presence of smear in the lanes indicative of complexes that dissociated during electrophoresis. The addition of MutSγ resulted in a moderate stabilization of the protein-DNA complex, and a minor super-shift in electrophoretic mobility of the stable protein-DNA band (indicated by the red and blue arrows). Shown are representative experiments. **b**, Electrophoretic mobility shift assays as in panel a, but without magnesium (with 3 mM EDTA). **c**, Quantitation of assays such as shown in panel b. The Y axis indicates relative protein-DNA complex stability, obtained upon dividing the protein-DNA band intensity (see blue or red arrows in panel b) by the intensity of the radioactive signal in the lane above the free substrate band, but below the protein-DNA band. Averages shown; error bars, SEM; n=5. **d**, Assays as in a, with human MutLγ and either human or yeast MutSγ. The supershift was observed only when the cognate human complexes were combined. **e**, Electrophoretic mobility shift assays as in a, but with yeast MutLγ and MutSγ complexes. **f**, Protein interaction assays with immobilized MLH1-MLH3 (bait) and MSH4-MSH5 (prey). The 10% polyacrylamide gel was stained with silver. **g**, Protein interaction assays with immobilized human MSH4-MSH5 or yeast Msh4-Msh5 that were used as baits, and human MLH1-MLH3 (prey). The eluted proteins were analyzed by silver staining. Although interaction between yeast Msh4-Msh5 and human MLH1-MLH3 was still detected, it was weaker than the interaction between the cognate MSH4-MSH5 and MLH1-MLH3 complexes. **h**, Protein interaction assay with immobilized yeast Msh4-Msh5 (bait) and yeast Mlh1-Mlh3 (prey). The

eluted proteins were analyzed by western blotting. **i**, Electrophoretic mobility shift assays with MLH1-MLH3 and MSH4-MSH5, as indicated, and oligonucleotide-based HJ DNA substrate. ^{32}P-labeled λDNA/*Hin*dIII digest was used as a marker. The DNA-bound MLH1-MLH3 and MSH4-MSH5 species migrate high up on the agarose gel where the resolution capacity is limited. **j**, Electrophoretic mobility shift assay with yeast Ku70-Ku80 heterodimer and HJ DNA substrate. Ku bound the dsDNA ends of the four HJ arms, resulting in up to 4 heterodimers bound to the DNA substrate (lanes 5-7). Comparison with λ DNA/*Hin*dIII and panel i revealed that the Ku-DNA complex migrates much faster than DNA-bound MLH1-MLH3 and MSH4-MSH5. This suggests that multiple units of MLH1-MLH3 and MSH4-MSH5 bind DNA.

Extended Data Figure 4. MSH4-MSH5 promotes DNA cleavage by MLH1-MLH3, but the complex does not exhibit resolvase activity. a, Quantitation of kinetic nuclease assays with MLH1-MLH3 (50 nM) without or with MSH4-MSH5 (50 nM) using 5.6 kbp-long scDNA. The assays were carried out at 30 °C in the presence of 5 mM manganese acetate and 2 mM ATP. Averages shown; error bars, SEM; n=3. **b**, Nuclease assays with MSH4-MSH5 and either wild type MLH1-MLH3 or nuclease-dead MLH1-MLH3 (D1223N-Q1224K-E1229K, 3ND). The assays were carried out at 30 °C in the presence of 5 mM manganese acetate and 0.5 mM ATP. **c**, Quantitation of nuclease assays with various MLH1-MLH3 and MSH4-MSH5 concentrations, as indicated. The assays were carried out at 30 °C in the presence of 5 mM manganese acetate and 0.5 mM ATP. Averages shown; error bars, SEM, n=3. The efficiency of nuclease cleavage was generally dependent on the concentrations used. When using 50 nM MLH1-MLH3, the maximal cleavage efficiency was achieved together with 50 nM MSH4-MSH5, no further increase when using 100 nM MSH4-MSH5 was observed. This suggests that both heterodimers may form a stoichiometric complex. *Vice versa*, when using 50 nM MSH4-MSH5, a further increase of DNA cleavage was observed when MLH1-MLH3 concentrations exceeded 50 nM, which is in agreement with the capacity of MLH1-MLH3 to cleave DNA on its own. **d**, Quantitation of nuclease assays with MLH1-MLH3 and MSH4-MSH5, as indicated, in the presence of various nucleotide cofactors or their analogs (2 mM). The assays were carried out at 30 °C in the

presence of 5 mM manganese acetate. Averages shown; error bars, SEM; n≥4. **e**, Representative nuclease assays with MSH4-MSH5 and variants of MLH1-MLH3 deficient in ATP hydrolysis, as indicated. The assays were carried out at 30 °C in the presence of 5 mM manganese acetate and 0.5 mM ATP. **f**, Representative nuclease assays with MLH1-MLH3 and variants of MSH4-MSH5 deficient in ATP hydrolysis, as indicated. The assays were carried out at 30 °C in the presence of 5 mM manganese acetate and 0.5 mM ATP. **g**, Recombinant MSH4-MSH5 and its variants used in this study. MSH4(G685A), MSH4(GA); MSH5(G597A), MSH5(GA). The 4-15% gradient polyacrylamide gel was stained with Coomassie Blue. **h**, Quantitation of electrophoretic mobility shift assays with MSH4-MSH5 and its ATPase motif mutant variants. Oligonucleotide-based HJ was used as the substrate. Asterisk (*) indicates the position of the radioactive label. ATP was not included in the binding buffer. The mutations did not affect the capacity of MSH4-MSH5 to bind DNA. Averages shown; error bars, SEM; n=3. **i**, Nuclease reactions were carried out with yeast or human MutSγ and MutLγ complexes, as indicated (50 nM), with 2.7 kbp-long scDNA substrate. While human MutSγ promoted DNA cleavage by human MutLγ (compare lanes 2 and 3), yeast MutSγ did not notably promote DNA cleavage by human MutLγ (compare lanes 2 and 5), and reciprocally, human MutSγ did not promote DNA cleavage by yeast MutLγ (compare lanes 7 and 8). **j**, Quantitation of nuclease assays with human and yeast MutSγ and MutLγ complexes as in panel i, but with 10.3 kbp-long scDNA substrate. **k**, Cleavage of pIRbke8mut cruciform DNA (inverted repeats folding back to form a Holliday junction structure) by MutSγ and MutLγ complexes. The quantitation below the lanes represents an average from two independent experiments. Simultaneous cleavage of both strands at the junction point would lead to linear DNA. No linear DNA was observed with MutSγ and MutLγ, indicating a lack of canonical resolvase activity. **l**, Representative nuclease assays with indicated proteins and oligonucleotide-based HJ DNA. Asterisk (*) indicates the position of the radioactive label. No DNA cleavage was observed, indicating a lack of structure-specific DNA cleavage activity on the oligonucleotide-based substrate. The products were analyzed by 15% denaturing polyacrylamide gel electrophoresis.

Extended Data Figure 5. MutSβ but not MutSα stimulates MutLγ to a similar extent as MutSγ. a, Recombinant MutSβ (MSH2-MSH3) used in this study. **b**, Recombinant MutSα (MSH2-MSH6) used in this study. **c**, Nuclease assays with MLH1-MLH3, MSH4-MSH5, and MSH2-MSH3 or MSH2-MSH6, as indicated. The assays were carried out at 30 °C in the presence of 5 mM manganese acetate and 0.5 mM ATP. A representative experiment is shown at the bottom, a quantitation (averages shown; n=3; error bars, SEM) at the top.

Extended Data Figure 6. Stimulation of the nuclease activity of MutSγ-MutLγ by EXO1(D173A). a, Recombinant EXO1(D173A), used in this study. The 4-15% gradient polyacrylamide gel was stained with Coomassie Blue. **b**, Nuclease assays with MLH1-MLH3 and MSH4-MSH5, as indicated, without (left) or with EXO1(D173A) (right). The assays were carried out at 30 °C in the presence of 5 mM manganese acetate and 0.5 mM ATP. A representative experiment is shown at the bottom, a quantitation (averages shown; n=3; error bars, SEM) at the top. **c**, Nuclease assays with MLH1-MLH3 and/or EXO1(D173A), as indicated. The assays were carried out at 30 °C in the presence of 5 mM manganese acetate and 0.5 mM ATP. A representative experiment is shown at the bottom, a quantitation (averages shown; n=4; error bars, SEM) at the top. EXO1(DA) does not promote the nuclease of MLH1-MLH3 alone. The limited DNA cleavage in lane 3 likely results from residual nuclease activity of EXO1(D173A) that becomes apparent at high protein concentrations (100 nM) in the presence of manganese. **d**, Quantitation of electrophoretic mobility shift assays with MLH1-MLH3, MSH4-MSH5 and EXO1(D173A), as indicated. The protein-DNA species were resolved in 1% agarose gels. Averages shown; error bars, SEM; n=5. EXO1(D173A) did not notably affect DNA binding of MLH1-MLH3 and MSH4-MSH5. **e**, Nuclease assays with MLH1-MLH3, MSH4-MSH5 with either human EXO1(D173A) or yeast Exo1(D173A), as indicated. The assays were carried out at 30 °C in the presence of 5 mM manganese acetate and 0.5 mM ATP. A representative experiment is shown at the bottom, a quantitation (averages shown; n=5; error bars, SEM) at the top. **f**, Nuclease assays with MLH1-MLH3, MSH2-MSH3 and EXO1(D173A), as indicated. The assays were carried out at 30 °C in the presence of 5 mM

manganese acetate and 0.5 mM ATP. A representative experiment is shown at the bottom, a quantitation (averages shown; n=3; error bars, SEM) at the top.

Extended Data Figure 7. RFC-PCNA promote the nuclease activity of the MutSγ-MutLγ-EXO1(DA) ensemble. a, Recombinant human and yeast RFC and PCNA used in this study. The 4-15% gradient polyacrylamide gel was stained with Coomassie Blue. **b**, Nuclease assays with scDNA and indicated proteins (all 50 nM, except human PCNA, 100 nM) were carried out with 5 mM magnesium acetate and 2 mM ATP at 37 °C. A representative experiment is shown at the bottom, a quantitation (averages shown; n≥4; error bars, SEM) at the top. **c**, Experiments as in panel b, comparing the efficacy of human and yeast RFC as a part of the MLH3 nuclease ensemble. Averages shown; n=4; error bars, SEM. **d**, Nuclease reactions containing MLH1-MLH3 (50 nM), MSH4-MSH5 (50 nM), EXO1(D173A) (50 nM) and yRFC-hPCNA (50-100 nM, respectively) (column 1), without MSH4-MSH5 (column 2) or without hEXO1(D173A) (column 3). Reactions were carried out with 5 mM magnesium acetate and 2 mM ATP at 37 °C. Averages shown; error bars, SEM; n≥4. **e**, Kinetic nuclease assays with MLH1-MLH3 (50 nM), MSH4-MSH5 (50 nM), EXO1(D173A) (50 nM) and yRFC-hPCNA (50-100 nM, respectively), as indicated. Reactions were carried out with 5 mM magnesium acetate and 2 mM ATP at 37 °C. Averages shown; error bars, SEM; n≥5. **f**, Nuclease assays with MLH1-MLH3 (50 nM), MSH4-MSH5 (50 nM), EXO1(D173A) (50 nM) and hRFC-hPCNA (50-100 nM, respectively), as indicated, with supercoiled (left) or relaxed DNA (right). Reactions were carried out with 5 mM magnesium acetate and 2 mM ATP at 37 °C. Shown is a representative experiment. RFC-PCNA do not stimulate the cleavage of relaxed DNA. **g**, Nuclease assays with MLH1-MLH3, MSH4-hMSH5, EXO1(D173A) without or with yRFC-hPCNA, as indicated. The assays were carried out at 37 °C in the presence of 5 mM manganese acetate and 2 mM ATP. A representative experiment is shown at the bottom, a quantitation (averages shown; n=3; error bars, SEM) at the top. Without magnesium, no stimulation of DNA cleavage by RFC-PCNA was observed. **h**, Nuclease reactions with MLH1-MLH3 (50 nM), MSH4-MSH5 (50 nM), EXO1(D173A) (50 nM) and yRFC-hPCNA (50-100 nM, respectively), as indicated. Reactions were carried out with 5 mM magnesium acetate and 2 mM ATP at 37 °C. Averages shown; error bars,

SEM; n≥5. **i**, Nuclease assays with MLH1-MLH3 (50 nM), MSH4-MSH5 (50 nM), EXO1(D173A) (50 nM) and yRFC-hPCNA (50-100 nM, respectively) and 5 mM magnesium acetate, either with no nucleotide co-factor (lane 2), with ATP (2 mM, lane 3) or ADP (2 mM, lane 4). ATP is strictly required for DNA cleavage by the nuclease ensemble. **j**, Representative nuclease assays with MLH1-MLH3 (50 nM), MSH4-MSH5 (50 nM), EXO1(D173A) (50 nM) and yRFC-hPCNA (50-100 nM, respectively), lane 2. Lanes 3-7 contain instead MLH1-MLH3 or MSH4-MSH5 variants deficient in ATP hydrolysis, as indicated. See Fig. 1d,e for the specific mutations. Reactions were carried out with 5 mM magnesium acetate and 2 mM ATP at 37 °C. Averages shown; error bars, SEM; n=4. **k**, Nuclease assays with indicated oligonucleotide-based substrates carried out at 37 °C in the presence of 5 mM manganese acetate and 2 mM ATP. All proteins 30 nM, as indicated. Asterisk (*) indicates the position of the radioactive label. The reaction products were analyzed on a 15% denaturing polyacrylamide gel. No DNA cleavage was observed.

Extended Data Figure 8. PIP box-like motifs in EXO1, MLH3 and MLH1 facilitate the stimulatory effect of RFC-PCNA on the hMLH3 nuclease ensemble. **a**, The MLH1^{P}-MLH3^{P} variant (see Fig. 3b) is not impaired in HJ-binding. Electrophoretic mobility shift assay was carried out with 5 ng/reaction dsDNA competitor and 3 mM EDTA (no magnesium). Asterisk (*) indicates the position of the radioactive label. **b**, The MLH1^{P} and MLH3^{P} variant combinations are not impaired in nuclease activity without or with MSH4-MSH5 and EXO1(D173A) in the absence of RFC-PCNA. The nuclease assays were performed with 5 mM manganese acetate and 2 mM ATP at 37 °C. Averages shown; error bars, SEM, n=3. **c**, Nuclease assays with MSH4-MSH5 (50 nM), EXO1(D173A) (50 nM) and yRFC-hPCNA (50-100 nM), and a respective MLH1-MLH3 variant, as indicated (see Fig. 3b). Mutations in the PIP-box like motif reduce the stimulation of the nuclease ensemble by RFC-PCNA. The assays were carried out with 5 mM magnesium acetate and 2 mM ATP at 37 °C. Averages shown; error bars, SEM, n=5. **d**, The EXO1^{P}(D173A) variant with mutated PIP-box motif (see Fig. 3b) is not affected in its ability to promote the nuclease of MLH1-MLH3 and MSH4-MSH5 (without RFC-PCNA). The assays were carried out with 5 mM manganese acetate and 2 mM ATP at 37 °C. Averages shown; error bars, SEM, n=4. **e**, The EXO1^{P}(D173A) variant

with mutated PIP-box motif (see Fig. 3b), in complex with MLH1-MLH3 and MSH4-MSH5 impairs the stimulatory function of yRFC-hPCNA (50-100 nM). The assays were carried out with 5 mM magnesium acetate and 2 mM ATP at 37 °C. Averages shown; error bars, SEM, n=5.

Extended Data Figure 9. RFC-PCNA promote meiotic recombination in yeast cells. a, Spore viability upon tetrad microdissection, analyzed in the wild type strain, *mlh1*Δ and *mlh3*Δ, and in strains complemented with a construct expressing untagged Mlh1^{P} (Q572A-L575A-F578A) or Mlh3^{P} (Q293A-V296A-F300A) at the endogenous chromosomal locus. At least 156 spores from 2 biological replicates were analyzed for each genotype. **b**, Western blot analysis of Mlh1^{P} expression in yeast. TCA extracts were prepared from exponentially proliferating SK1 strains expressing *MLH1*, *MLH1-FLAG or MLH1*^{P}*-FLAG* from the endogenous gene locus. The PIP-box-like mutation affects the stability of the FLAG-tagged Mlh1 protein. Blots were probed with anti-FLAG antibody (Sigma, F7425). Crm1 is a protein normalization control. Asterisk denotes a cross-reacting band. **c**, Western blot analysis of Mlh3^{P} expression in yeast. As in b, but with *MLH3*, *MLH3-FLAG* or *MLH3*^{P}*-FLAG* constructs. Blots were probed with anti-FLAG antibodies: Sigma F7425 (left panel); A8592 (right panel). Crm1 is a protein normalization control. Mlh1-FLAG and Mlh3^{P}-FLAG showed comparable expression levels. Asterisks denote cross-reacting bands. **d**, A pulldown of TAP-tagged yeast Rfc1-5 and associated proteins from meiotic cell extracts from p*CUP1-IME1* cells 5 h 30 min after the induction of meiosis. The presence of Mlh1-HA and Mlh3-Myc in the TEV eluate was analyzed by Western blotting. **e**, Rfc1-TAP levels at the three indicated meiotic DSB hotspots relative to a negative control site (*NFT1)* were assessed by ChIP and qPCR in *ndt80Δ*-arrested cells after 7 h in meiosis. Mlh3 is not required for the recruitment of RFC to the meiotic DSB hotspots. *MLH3*: VBD2136; *mlh3Δ*: VBD2137. Averages show; error bars, SD, n = 2.

Extended Data Figure 10. A possible model for biased resolution of recombination intermediates by the MLH3 nuclease ensemble. Meiotic dsDNA breaks (a) are resected (1) and the resulting DNA overhang invades matching

DNA on a homologous chromosome (2). The unstable D-Loop intermediates (b) are stabilized by MSH4-MSH5 (3), DNA synthesis by RFC-PCNA-Polδ (4) and branch migration (5), leading to more stable structures termed single-end invasions (c). This is followed by a second end capture (6), and more DNA synthesis (7) leading to precursors of double Holliday junctions (d) and later matured double Holliday junctions (e). As a result of the previous steps, MSH4-MSH5 and RFC-PCNA may be present asymmetrically at the (d) or (e) intermediates at the junctions points or their vicinity. The asymmetric presence of the co-factors then directs and stimulates the biased DNA cleavage (9) of (d) or (e) structures by MLH1-MLH3-EXO1. Upon final processing (10) and ligation (11), the ultimate result is a DNA crossover characterized by reciprocal exchange of the DNA arms of the recombining chromosomes.

Figure 1

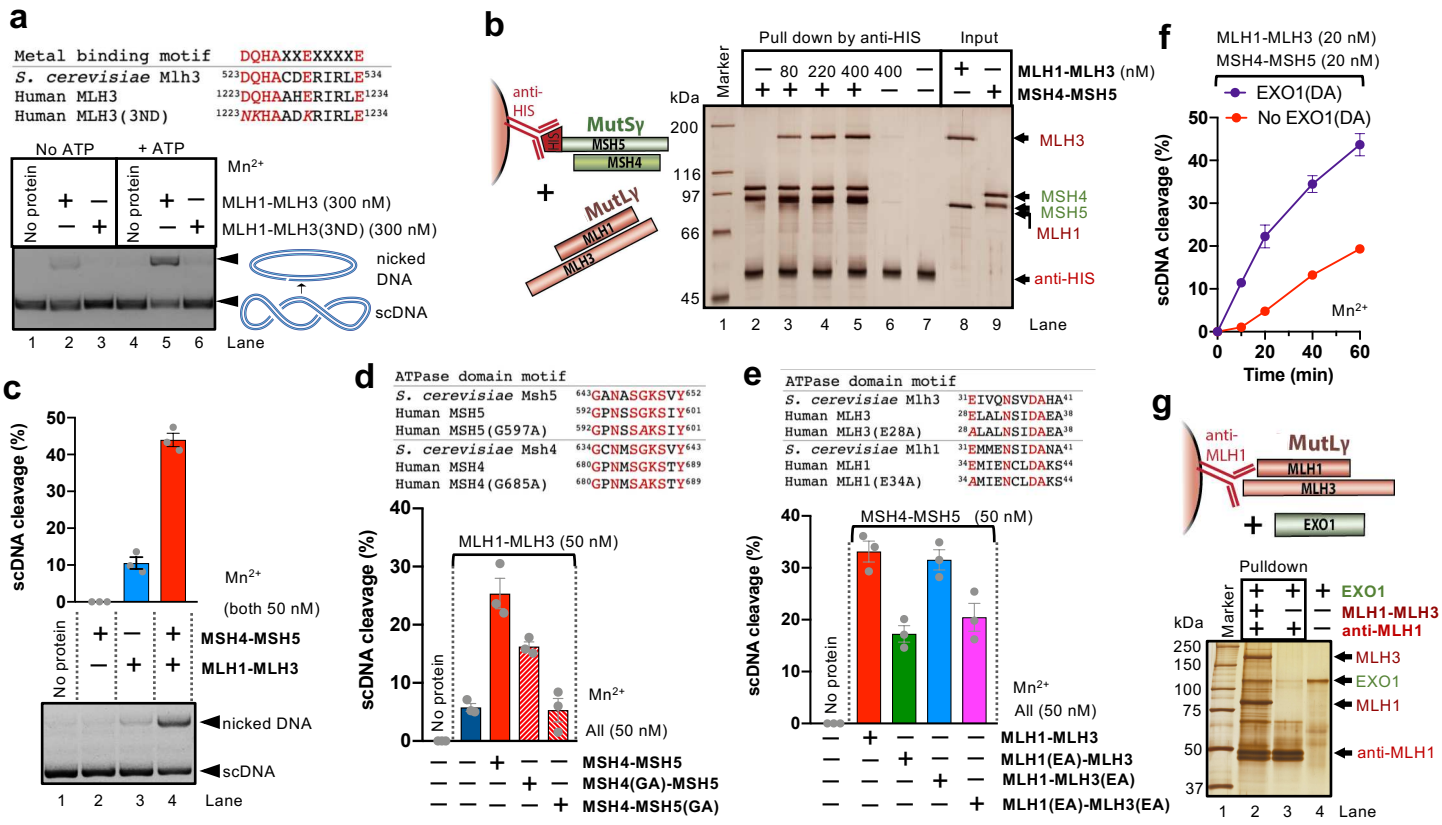
a
Metal binding motif DQHAXXEXXXXE
S. cerevisiae Mlh3 523DQHACDERIRLE534
Human MLH3 1223DQHAAHERIRLE1234
Human MLH3(3ND) 1223NKHAADKRIRLE1234
No ATP
+ ATP
Mn2+
No protein
MLH1-MLH3 (300 nM)
MLH1-MLH3(3ND) (300 nM)
nicked DNA
scDNA
1 2 3 4 5 6 Lane
b
anti-HIS
MutSγ
MSH5
MSH4
MutLγ
MLH1
MLH3
Pull down by anti-HIS
Input
Marker
kDa
200
116
97
66
45
80 220 400 400
MLH1-MLH3 (nM)
MSH4-MSH5
MLH3
MSH4
MSH5
MLH1
anti-HIS
1 2 3 4 5 6 7 8 9 Lane
f
MLH1-MLH3 (20 nM)
MSH4-MSH5 (20 nM)
EXO1(DA)
No EXO1(DA)
scDNA cleavage (%)
Mn2+
Time (min)
c
scDNA cleavage (%)
Mn2+
(both 50 nM)
No protein
MSH4-MSH5
MLH1-MLH3
nicked DNA
scDNA
1 2 3 4 Lane
d
ATPase domain motif
S. cerevisiae Msh5 643GANASGKSVY652
Human MSH5 592GPNSSGKSIY601
Human MSH5(G597A) 592GPNSSAKSIY601
S. cerevisiae Msh4 634GCNMSGKSVY643
Human MSH4 680GPNMSGKSTY689
Human MSH4(G685A) 680GPNMSAKSTY689
MLH1-MLH3 (50 nM)
scDNA cleavage (%)
No protein
Mn2+
All (50 nM)
MSH4-MSH5
MSH4(GA)-MSH5
MSH4-MSH5(GA)
e
ATPase domain motif
S. cerevisiae Mlh3 31EIVQNSVDAHA41
Human MLH3 28ELALNSIDAEA38
Human MLH3(E28A) 28ALALNSIDAEA38
S. cerevisiae Mlh1 31EMMENSIDANA41
Human MLH1 34EMIENCLDAKS44
Human MLH1(E34A) 34AMIENCLDAKS44
MSH4-MSH5 (50 nM)
scDNA cleavage (%)
No protein
Mn2+
All (50 nM)
MLH1-MLH3
MLH1(EA)-MLH3
MLH1-MLH3(EA)
MLH1(EA)-MLH3(EA)
g
anti-MLH1
MutLγ
MLH1
MLH3
EXO1
Pulldown
Marker
kDa
250
150
100
75
50
37
EXO1
MLH1-MLH3
anti-MLH1
MLH3
EXO1
MLH1
anti-MLH1
1 2 3 4 Lane

Figure 2

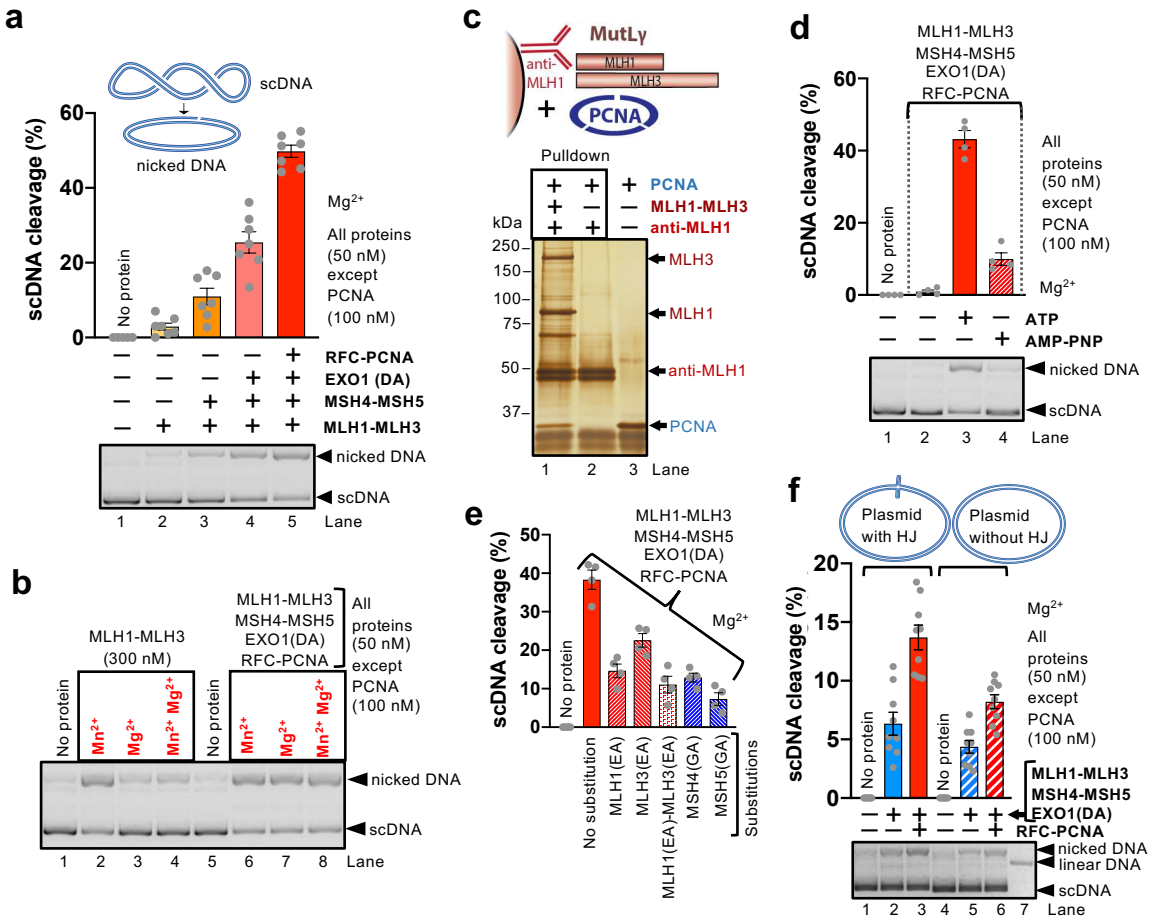
a
scDNA
nicked DNA
scDNA cleavage (%)
60
40
20
0
No protein
Mg2+
All proteins (50 nM) except PCNA (100 nM)
RFC-PCNA
EXO1 (DA)
MSH4-MSH5
MLH1-MLH3
nicked DNA
scDNA
1 2 3 4 5 Lane
b
MLH1-MLH3 (300 nM)
MLH1-MLH3 MSH4-MSH5 EXO1(DA) RFC-PCNA
All proteins (50 nM) except PCNA (100 nM)
No protein
Mn2+
Mg2+
Mn2+ Mg2+
nicked DNA
scDNA
1 2 3 4 5 6 7 8 Lane
c
MutLγ
anti-MLH1
MLH1
MLH3
PCNA
Pulldown
PCNA
MLH1-MLH3
anti-MLH1
kDa
250
150
100
75
50
37
MLH3
MLH1
anti-MLH1
PCNA
1 2 3 Lane
d
MLH1-MLH3
MSH4-MSH5
EXO1(DA)
RFC-PCNA
scDNA cleavage (%)
60
40
20
0
No protein
All proteins (50 nM) except PCNA (100 nM)
Mg2+
ATP
AMP-PNP
nicked DNA
scDNA
1 2 3 4 Lane
e
MLH1-MLH3
MSH4-MSH5
EXO1(DA)
RFC-PCNA
Mg2+
scDNA cleavage (%)
50
40
30
20
10
0
No protein
No substitution
MLH1(EA)
MLH3(EA)
MLH1(EA)-MLH3(EA)
MSH4(GA)
MSH5(GA)
Substitutions
f
Plasmid with HJ
Plasmid without HJ
scDNA cleavage (%)
20
15
10
5
0
No protein
Mg2+
All proteins (50 nM) except PCNA (100 nM)
MLH1-MLH3
MSH4-MSH5
EXO1(DA)
RFC-PCNA
nicked DNA
linear DNA
scDNA
1 2 3 4 5 6 7 Lane

Figure 3

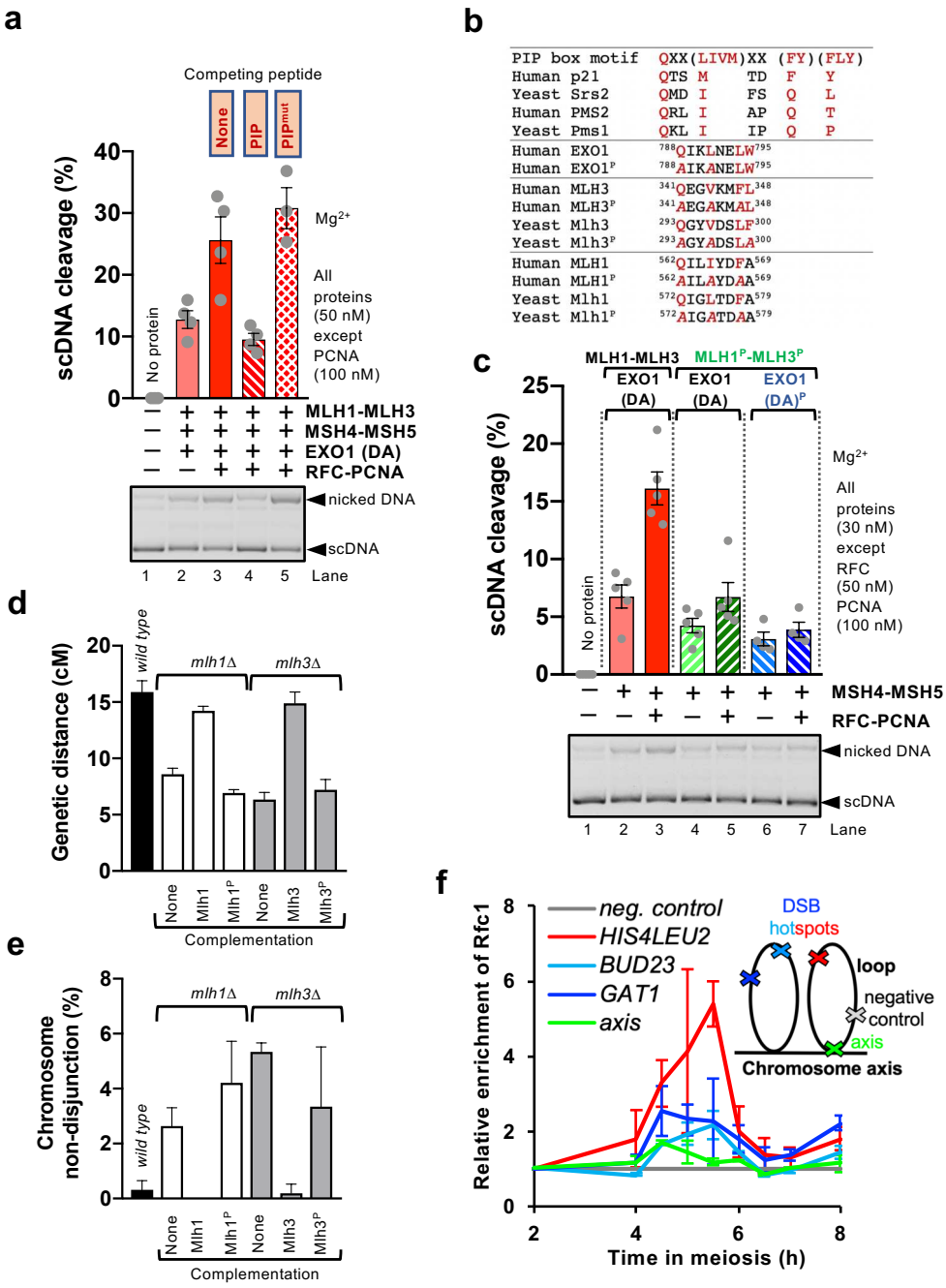
a
Competing peptide
None
PIP
PIPmut
scDNA cleavage (%)
No protein
Mg2+
All proteins (50 nM) except PCNA (100 nM)
MLH1-MLH3
MSH4-MSH5
EXO1 (DA)
RFC-PCNA
nicked DNA
scDNA
Lane
b
PIP box motif QXX(LIVM)XX (FY)(FLY)
Human p21 QTS M TD F Y
Yeast Srs2 QMD I FS Q L
Human PMS2 QRL I AP Q T
Yeast Pms1 QKL I IP Q P
Human EXO1 788QIKLNELW795
Human EXO1P 788AIKANELW795
Human MLH3 341QEGVKMFL348
Human MLH3P 341AEGAKMAL348
Yeast Mlh3 293QGYVDSLF300
Yeast Mlh3P 293AGYADSLA300
Human MLH1 562QILIYDFA569
Human MLH1P 562AILAYDAA569
Yeast Mlh1 572QIGLTDFA579
Yeast Mlh1P 572AIGATDAA579
c
MLH1-MLH3
MLH1P-MLH3P
EXO1 (DA)
EXO1 (DA)
EXO1 (DA)P
scDNA cleavage (%)
No protein
Mg2+
All proteins (30 nM) except RFC (50 nM) PCNA (100 nM)
MSH4-MSH5
RFC-PCNA
nicked DNA
scDNA
Lane
d
Genetic distance (cM)
wild type
mlh1Δ
mlh3Δ
None
Mlh1
Mlh1P
None
Mlh3
Mlh3P
Complementation
e
Chromosome non-disjunction (%)
wild type
mlh1Δ
mlh3Δ
None
Mlh1
Mlh1P
None
Mlh3
Mlh3P
Complementation
f
Relative enrichment of Rfc1
neg. control
HIS4LEU2
BUD23
GAT1
axis
DSB hotspots
loop
negative control
axis
Chromosome axis
Time in meiosis (h)

Extended Data Figure 1

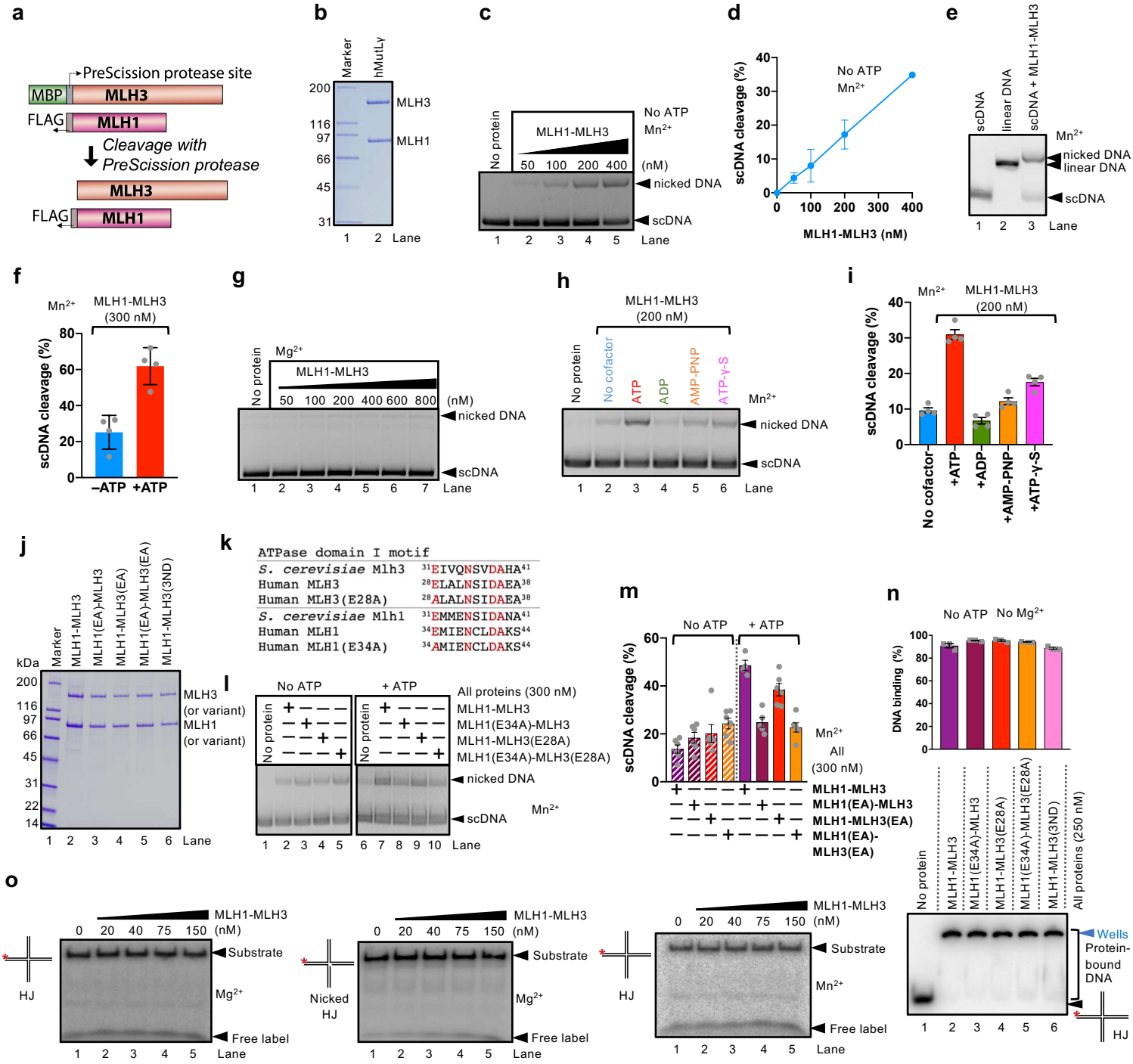

Extended Data Figure 2

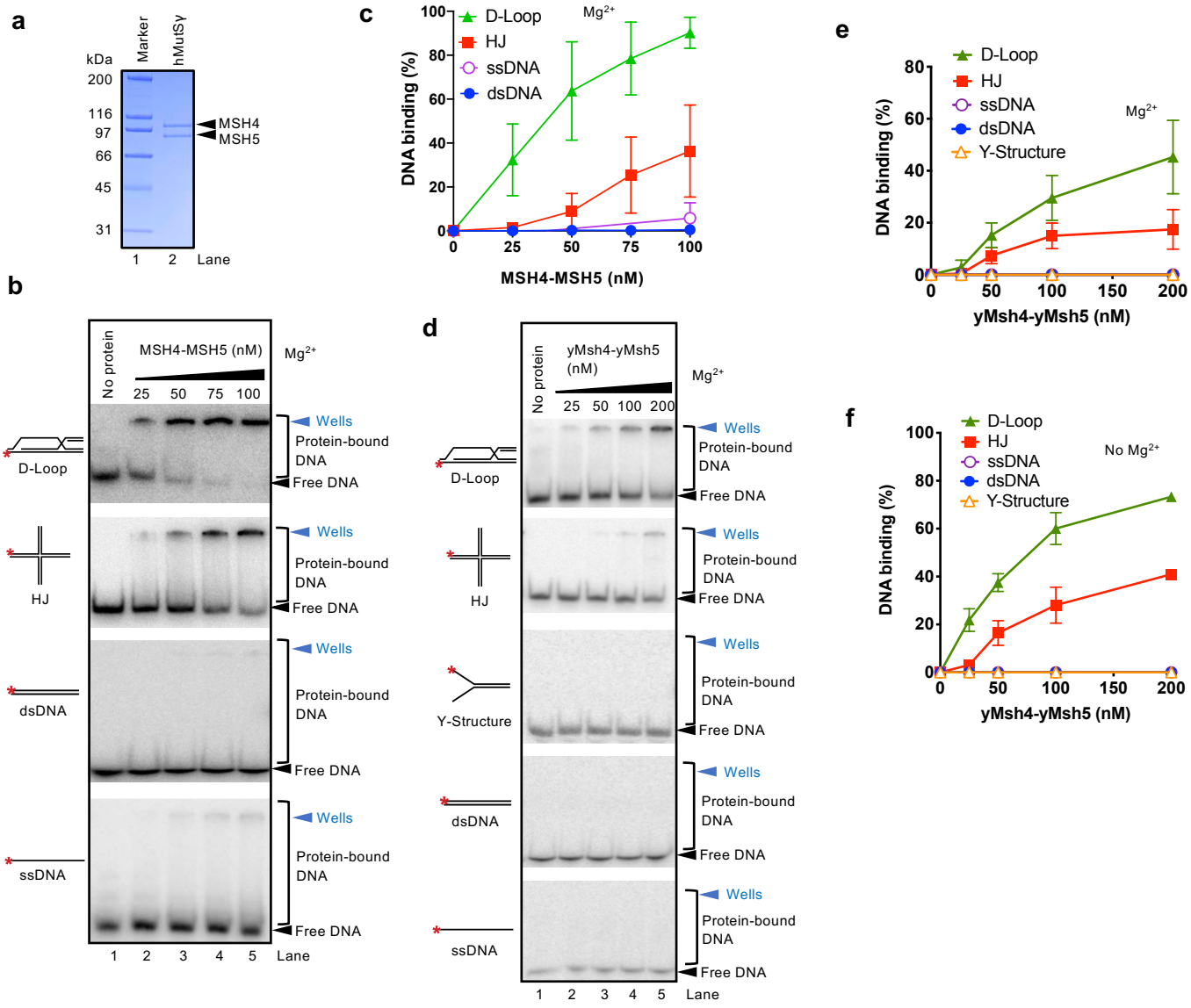

Extended Data Figure 3

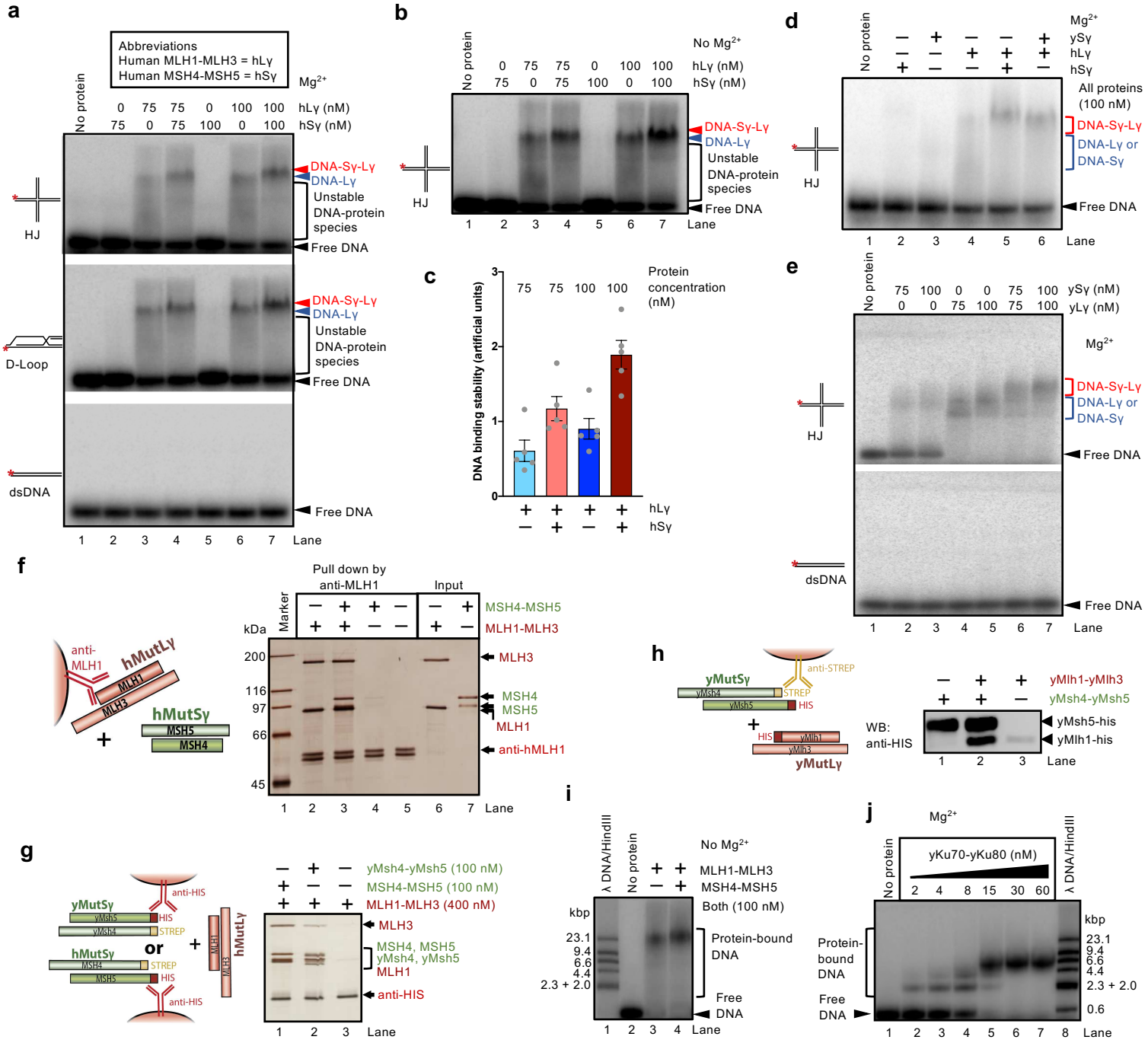

Extended Data Figure 4

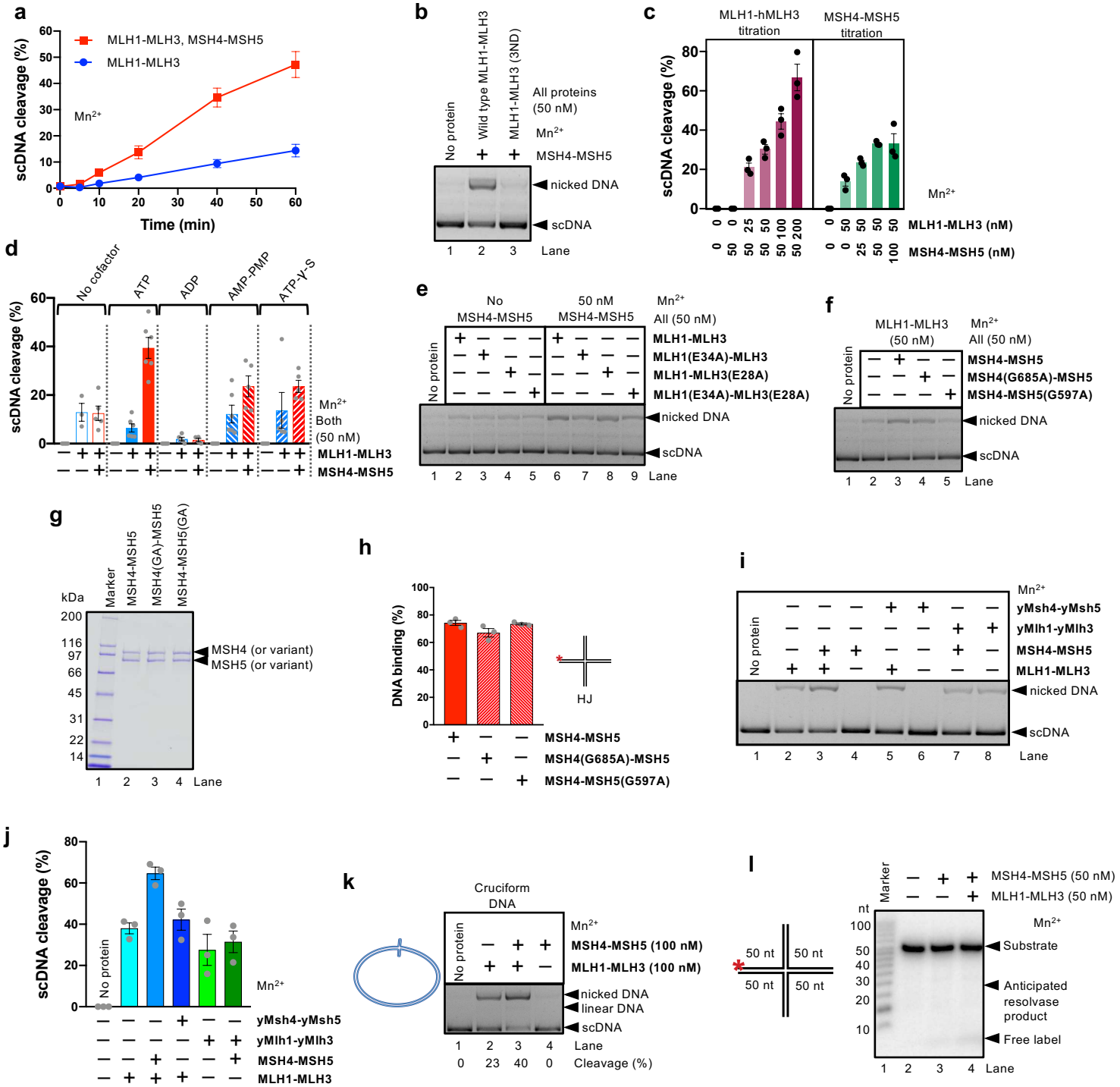

Extended Data Figure 5

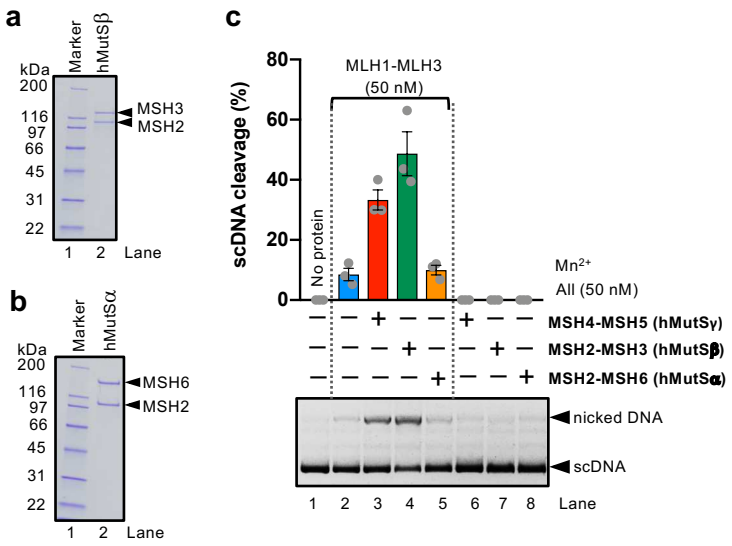

Extended Data Figure 6

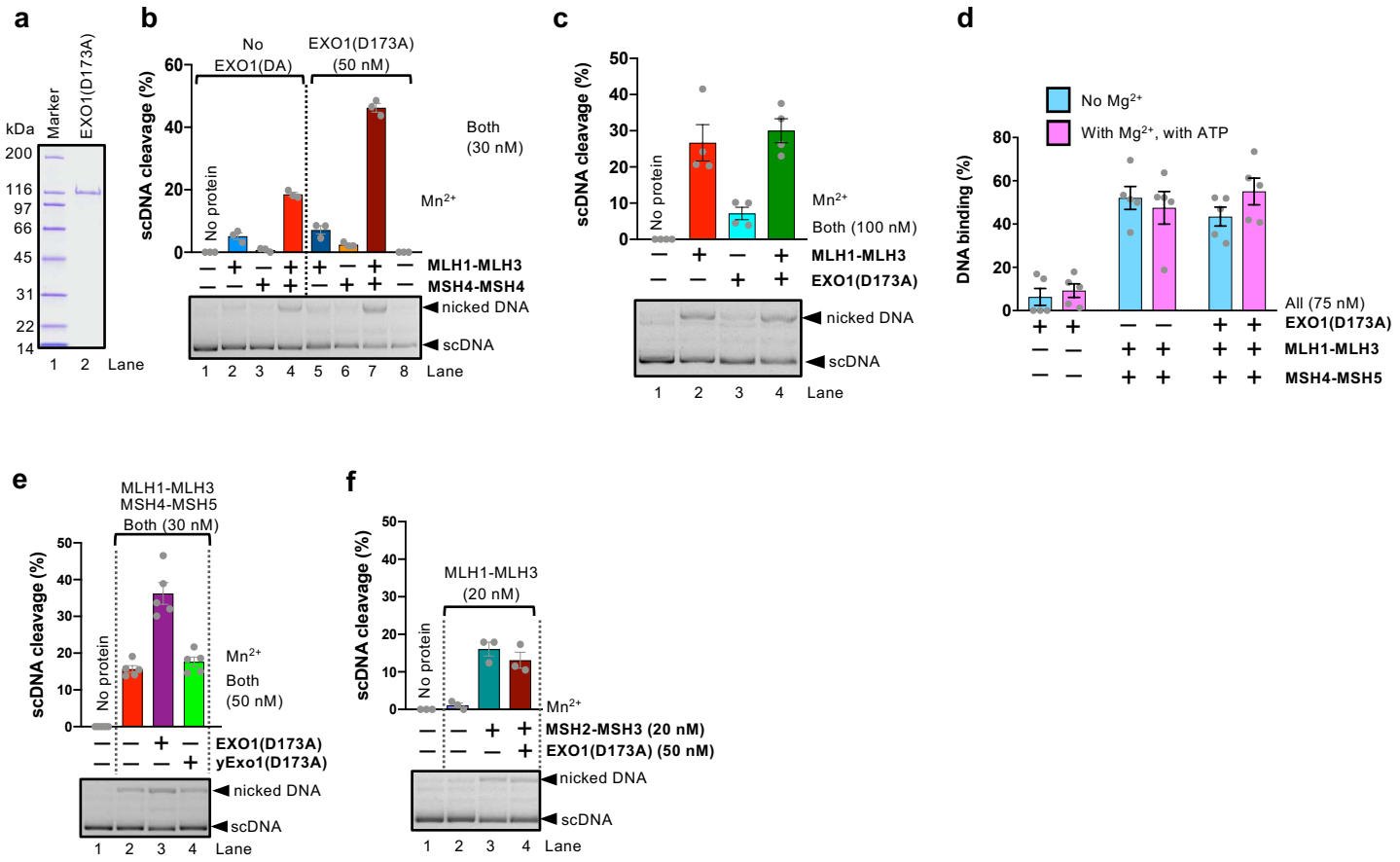

Extended Data Figure 7

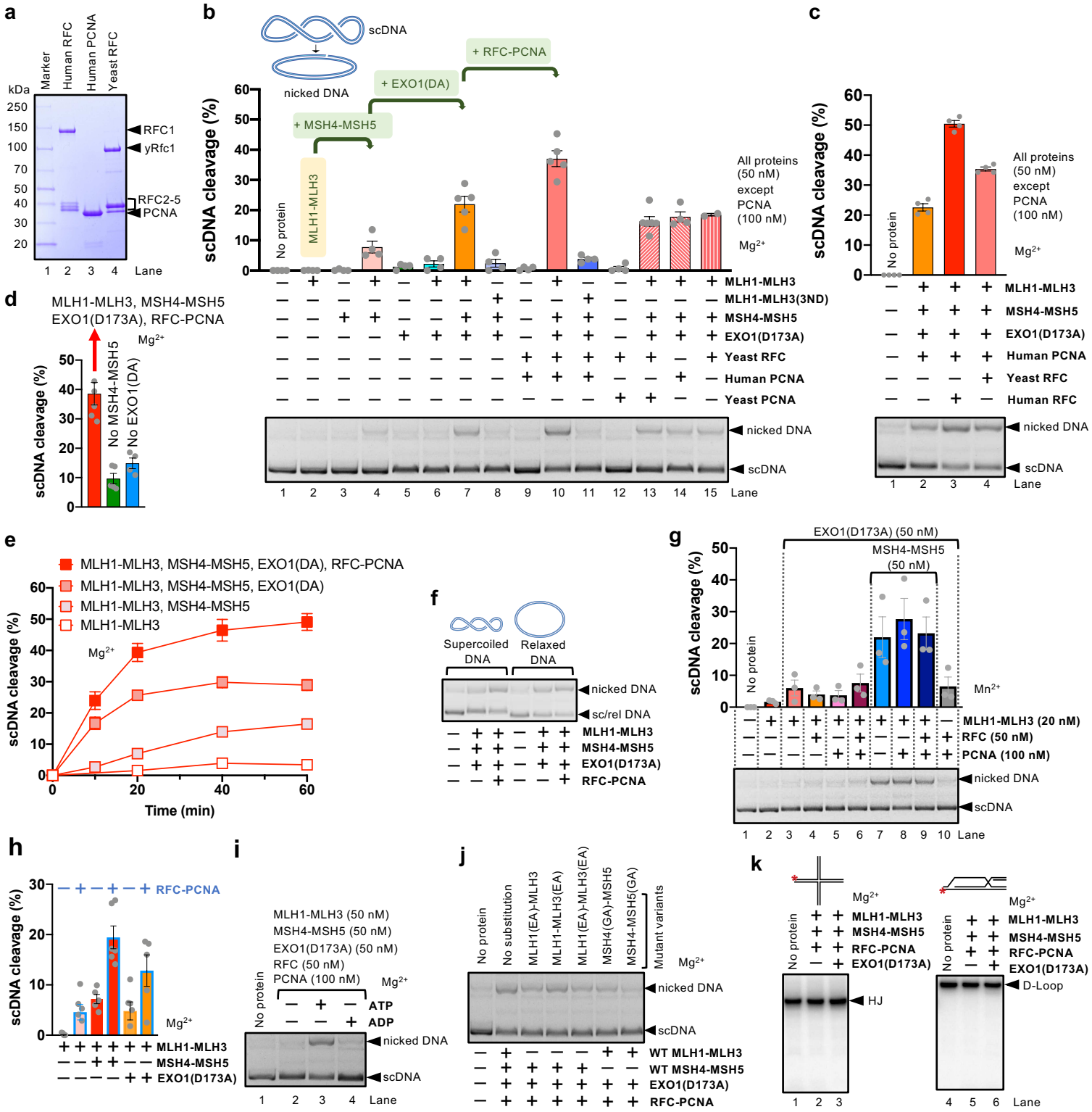

Extended Data Figure 8

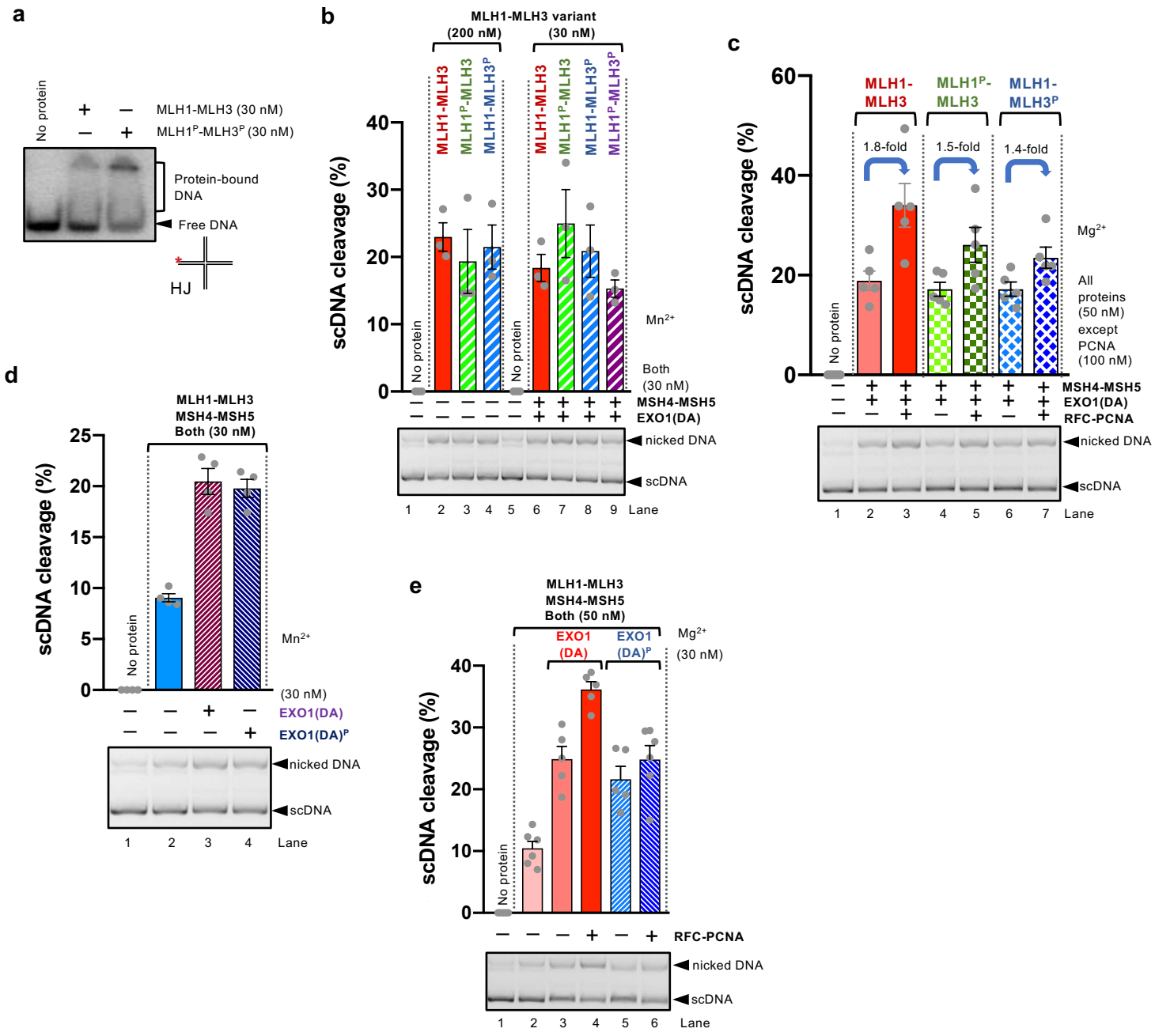

Extended Data Figure 9

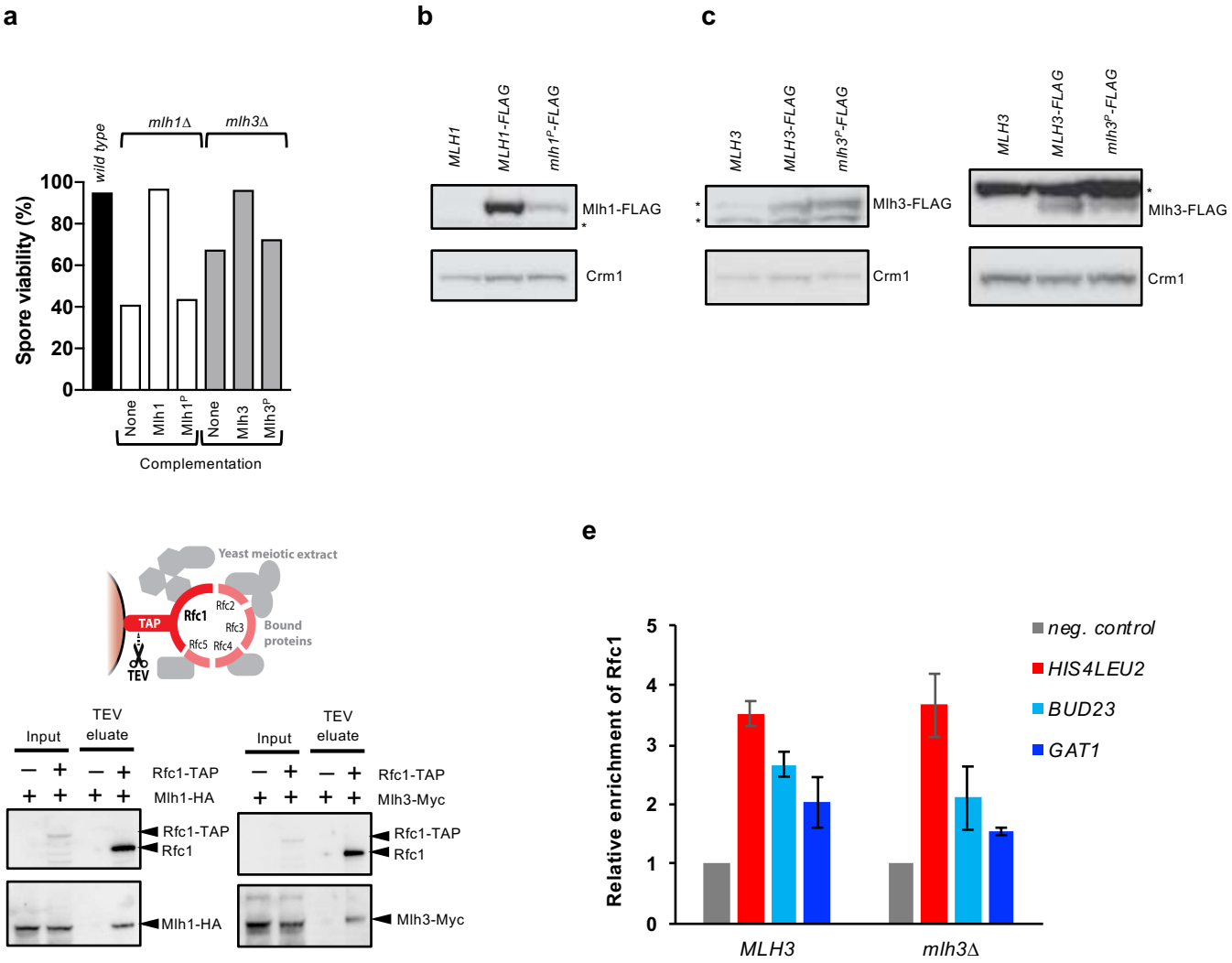

Extended Data Figure 10